

- heterophil Hanganutziu-Deicher antigens. *Immunol Lett* **32**, 91, 1992.
25. Matsuyama, A., Yamashita, S., Sakai, N., Maruyama, T., Okuda, E., Hirano, K., Kihara, S., Hiraoka, H., and Matsuzawa, Y. Identification of a GPI-anchored type HDL-binding protein on human macrophages. *Biochem Biophys Res Commun* **272**, 864, 2000.
 26. Hashikawa, T., Takedachi, M., Terakura, M., Yamada, S., Thompson, L.F., Shimabukuro, Y., and Murakami, S. Activation of adenosine receptor on gingival fibroblasts. *J Dent Res* **85**, 739, 2006.
 27. Labarca, C., and Paigen, K. A simple, rapid, and sensitive DNA assay procedure. *Anal Biochem* **102**, 344, 1980.
 28. Schaapherder, A.F., Daha, M.R., te Bulte, M.T., van der Woude, F.J., and Gooszen, H.G. Antibody-dependent cell-mediated cytotoxicity against porcine endothelium induced by a majority of human sera. *Transplantation* **57**, 1376, 1994.
 29. Ezzelarab, M., Ayares, D., and Cooper, D.K. Carbohydrates in xenotransplantation. *Immunol Cell Biol* **83**, 396, 2005.
 30. Yang, Y.G., and Sykes, M. Xenotransplantation: current status and a perspective on the future. *Nat Rev Immunol* **7**, 519, 2007.
 31. Roos, A., and Daha, M.R. Antibody-mediated activation of the classical complement pathway in xenograft rejection. *Transpl Immunol* **9**, 257, 2002.
 32. Miyagawa, S., Kubo, T., Matsunami, K., Kusama, T., Beppu, K., Nozaki, H., Moritan, T., Ahn, C., Kim, J.Y., Fukuta, D., and Shirakura, R. Delta-short consensus repeat 4-decay accelerating factor (DAF: CD55) inhibits complement-mediated cytolysis but not NK cell-mediated cytolysis. *J Immunol* **173**, 3945, 2004.
 33. Komoda, H., Miyagawa, S., Kubo, T., Kitano, E., Kitamura, H., Omori, T., Ito, T., Matsuda, H., and Shirakura, R. A study of the xenoantigenicity of adult pig islets cells. *Xenotransplantation* **11**, 237, 2004.
 34. Diamond, L.E., Quinn, C.M., Martin, M.J., Lawson, J., Platt, J.L., and Logan, J.S. A human CD46 transgenic pig model system for the study of discordant xenotransplantation. *Transplantation* **71**, 132, 2001.
 35. Schuurman, H.J., Pino-Chavez, G., Phillips, M.J., Thomas, L., White, D.J., and Cozzi, E. Incidence of hyperacute rejection in pig-to-primate transplantation using organs from hDAF-transgenic donors. *Transplantation* **73**, 1146, 2002.
 36. Zhou, C.Y., McInnes, E., Copeman, L., Langford, G., Parsons, N., Lancaster, R., Richards, A., Carrington, C., and Thompson, S. Transgenic pigs expressing human CD59, in combination with human membrane cofactor protein and human decay-accelerating factor. *Xenotransplantation* **12**, 142, 2005.
 37. Chen, G., Qian, H., Starzl, T., Sun, H., Garcia, B., Wang, X., Wise, Y., Liu, Y., Xiang, Y., Copeman, L., Liu, W., Jevnikar, A., Wall, W., Cooper, D.K., Murase, N., Dai, Y., Wang, W., Xiong, Y., White, D.J., and Zhong, R. Acute rejection is associated with antibodies to non-Gal antigens in baboons using Gal-knockout pig kidneys. *Nat Med* **11**, 1295, 2005.
 38. Chen, G., Sun, H., Yang, H., Kubelik, D., Garcia, B., Luo, Y., Xiang, Y., Qian, A., Copeman, L., Liu, W., Cardella, C.J., Wang, W., Xiong, Y., Wall, W., White, D.J., and Zhong, R. The role of anti-non-Gal antibodies in the development of acute humoral xenograft rejection of hDAF transgenic porcine kidneys in baboons receiving anti-Gal antibody neutralization therapy. *Transplantation* **81**, 273, 2006.
 39. Saethre, M., Baumann, B.C., Fung, M., Seebach, J.D., and Mollnes, T.E. Characterization of natural human anti-nongal antibodies and their effect on activation of porcine gal-deficient endothelial cells. *Transplantation* **84**, 244, 2007.
 40. Ide, K., Ohdan, H., Kobayashi, T., Hara, H., Ishiyama, K., and Asahara, T. Antibody- and complement-independent phagocytotic and cytolytic activities of human macrophages toward porcine cells. *Xenotransplantation* **12**, 181, 2005.
 41. Yamaguchi, M., Hirayama, F., Wakamoto, S., Fujihara, M., Murahashi, H., Sato, N., Ikebuchi, K., Sawada, K., Koike, T., Kuwabara, M., Azuma, H., and Ikeda, H. Bone marrow stromal cells prepared using AB serum and bFGF for hematopoietic stem cells expansion. *Transfusion* **42**, 921, 2002.

Address correspondence to:

Akifumi Matsuyama, M.D., Ph.D.

Department of Somatic Stem Cell Therapy

Institute of Biomedical Research and Innovation

Foundation for Biomedical Research and Innovation

1-5-4 TRI 305

Minatojima-Minamimachi

Chuo-ku

Kobe 650-0047

Japan

E-mail: akifumi-matsuyama@umin.ac.jp

Received: June 9, 2009

Accepted: October 27, 2009

Online Publication Date: December 18, 2009

ORIGINAL ARTICLE

Suppressive effects of nicotine on the cytodifferentiation of murine periodontal ligament cells

M Yanagita, Y Kojima, T Kawahara, T Kajikawa, H Oohara, M Takedachi, S Yamada, S Murakami

Department of Periodontology, Division of Oral Biology and Disease Control, Osaka University Graduate School of Dentistry, Osaka, Japan

OBJECTIVES: Tobacco smoking has been suggested to be one of the important risk factors of developing periodontal disease. Although epidemiological studies have shown the detrimental effects of smoking on periodontal disease, the effects of smoke compounds on gingival tissue are not well understood. The aim of this study was to evaluate the effects of nicotine, which is the major component of the thousands of chemicals that constitute cigarette smoke, for cytodifferentiation of murine periodontal ligament (MPDL) cell.

MATERIALS AND METHODS: Expression of nAChR subunits on MPDL cells was examined using RT-PCR. The effects of nicotine on gene expression of extracellular matrices and osteoblastic transcription factors were evaluated by quantitative RT-PCR. Mineralized nodule formation of nicotine-treated MPDL cells was characterized by alizarin red staining.

RESULTS: Murine periodontal ligament cells expressed several subunits of nAChR, which have functional calcium signals in response to nicotine. Gene expression of extracellular matrices and osteoblastic transcription factors were reduced in nicotine-treated MPDL cells. In addition, mineralized nodule formation was inhibited in MPDL cells in the presence of nicotine.

CONCLUSION: Our findings indicate that nicotine may negatively regulate the cytodifferentiation and mineralization of MPDL cells.

Oral Diseases (2010) 16, 812–817

Keywords: periodontal ligament cells; nicotine; cytodifferentiation; mineralization

Introduction

The periodontal ligament (PDL) is a connective tissue that surrounds the root of the tooth and attaches the

root to the alveolar bone to provide mechanical support. The PDL also plays a nutritive and sensory role. In addition, PDL is regarded as a reservoir of multipotential mesenchymal stem cells that can differentiate into mineralized tissue-forming cells, such as osteoblasts and cementoblasts (Seo *et al*, 2004), and plays an important role in periodontal tissue remodeling and regeneration.

Cigarette smoking is known to be one of the most important risk factors in periodontal disease (Martinez-Canut *et al*, 1996; Ryder, 2007). Previous reports have shown that more clinical attachment loss and alveolar bone loss have been observed in smokers than in non-smokers (Grossi *et al*, 1994; Grossi *et al*, 1995). Tobacco smoke consists of thousands of chemicals (Lofroth, 1989) which individually, and collectively, can affect periodontal tissue. Nicotine is the main component of tobacco smoke and a selective agonist of the nicotinic acetylcholine receptor (nAChR). The main route of nicotine exposure is via inhalation of tobacco smoke. During inhalation, a high dose of nicotine (in excess of 10^{-3} M) would be exposed to the epithelial surface of the oral cavity, the bronchus and the lungs (Feyerabend *et al*, 1982; Seow *et al*, 1994). In particular, nicotine concentrations in the saliva of long-term snuff users can reach 9.6 mM (Hoffmann and Adams, 1981; Sato *et al*, 2008).

Therefore, we hypothesized that nicotine affects the characteristics of PDL directly and has detrimental effects on periodontal tissue, such as disease progression and the ineffectiveness for periodontal treatment. In this study, we investigated the gene expression of nAChR subunits and calcium influx via these receptors using a PDL clone obtained from murine PDL (MPDL) tissue (Yamada *et al*, 2007). We then examined the gene expression of alkaline phosphatase (ALP), collagen type I, bone sialoprotein (BSP), osterix, and runx2 in nicotine-treated MPDL. Further, the effects of nicotine on mineralization in MPDL were evaluated.

Materials and methods

Culture of MPDL

We have established a murine PDL clone cell, MPDL22, isolated from the PDL tissue of the molar teeth extracted from 2.5-week-old BALB/c mice (Yamada

Correspondence: Dr S Murakami, Department of Periodontology, Division of Oral Biology and Disease Control, Osaka University Graduate School of Dentistry, 1-8 Yamadaoka, Suita, Osaka 565-0871, Japan. Tel: +81 6 6879 2930, Fax: +81 6 6879 2934, E-mail: ipshinya@dent.osaka-u.ac.jp

Received 3 January 2010; revised 7 February 2010; accepted 17 February 2010

et al, 2007). MPDL22 cells were maintained in α -MEM (Nikken, Kyoto, Japan) supplemented with 10% fetal calf serum (FCS; JRH Biosciences, Lenexa, KS, USA) and 100 ng ml⁻¹ fibroblast growth factor-2 (FGF-2; Kaken, Kyoto, Japan) at 37°C in a humidified atmosphere of 5% CO₂. After the cells reached confluence, we replaced the culture medium (α -MEM supplemented with 10% FCS and FGF-2) with the mineralization medium (α -MEM supplemented with 10% FCS, 10 mM β -glycerophosphate, and 50 μ g ml⁻¹ ascorbic acid). We replaced the mineralization medium every 2 days with or without nicotine (10⁻⁸ M to 10⁻³ M), which was prepared in PBS and neutralized to pH 7.2.

Detection of nAChRs in MPDL by RT-PCR

MPDL22 cells were seeded at a density of 10⁵ cells per dish in 60 mm dishes and grown to confluency. Following the culture of MPDL cells, total RNA was extracted using the RNasee (TEL-TEST, Friendswood, TX, USA), according to the manufacturer's instructions. cDNA synthesis and amplification via PCR were performed, as described previously (Yamada *et al*, 2007). The primers used for PCR were prepared according to published results (Kageyama-Yahara *et al*, 2008). After denaturation at 94°C for 5 min, each PCR cycle consisted of 94°C for 30 s, 60°C for 45 s and 68°C for 45 s. Amplified products were analyzed by electrophoresis at 100 V for 30 min on 1.5% TAE agarose gels containing 0.5 μ g ml⁻¹ ethidium bromide. Murine brain samples were used as a positive control for nAChR subunits.

RT-PCR for ALP, collagen type I, BSP, osterix and runx2 mRNA

RNA samples were obtained from MPDL22 cells in α -MEM containing 1% FCS 2 days after nicotine treatment (10⁻³ M). Total RNA extract (0.4 mg) was reverse-transcribed using the High Capacity cDNA Reverse Transcriptase kit (Applied Biosystems, Foster City, CA, USA) to generate the single-stranded cDNA. PCRs were carried out using the ABI 7300 Fast Real-Time PCR System (Applied Biosystems) with Power SYBR^R Green PCR Master Mix (Applied Biosystems) according to the manufacturer's protocol. All reactions were run in triplicate. The primer sequences used for RT-PCR were as follows; ALP, (sense) 5'-ACA CCT GAC TGT GGT TAC TGC TGA-3', (antisense) 5'-CCT TGT AGC CAG GCC CGT TA-3'; collagen type I, (sense) 5'-ATG CCG CGA CCT CAA GAT G-3', (antisense) 5'-TGA GGC ACA GAC GGC TGA GTA-3'; BSP, (sense) 5'-TGG AGA CTG CGA TAG TTC CGA AG-3', (antisense) 5'-CGT AGC TAG CTG TTA CAC CCG AGA G-3'; Osterix, (sense) 5'-CGC ATC TGA AAG CCC ACT TG-3', (antisense) 5'-CAG CTC GTC AGA GCG AGT GAA-3'; runx2, (sense) 5'-CAC TGG CGG TGC AAC AAG A-3', (antisense) 5'-TTT CAT AAC AGC GGA GGC ATT TC-3'.

Proliferation assay

MPDL22 (5 \times 10³ cells per well) were incubated in 96-well plates in α -MEM containing 1% FCS in the

presence of nicotine or FGF-2 (100 ng ml⁻¹) for 48 h. Cell proliferation was measured using the non-radioactive colorimetric assay WST-1 system (Roche Diagnostics GmbH, Penzberg, Germany) according to the manufacturer's instructions and the OD450/650 measured after 2 h on a microplate reader (Bio-Rad, Hercules, CA, USA).

Intracellular calcium determination

The cells (2 \times 10⁴ cells per well) were incubated onto 96-well plates for 24 h and washed in PBS containing 1 mM Ca²⁺, 1 mM MgCl₂ and 0.1% bovine serum albumin (BSA). Cells were incubated with 200 μ l of 1 mg ml⁻¹ Fluo3-AM (Dojindo, Kumamoto, Japan) for 30 min in the dark. Cells were then rinsed three times in PBS wash solution, as described above, to remove any extra Fluo3-AM. Cells were stimulated with nicotine and levels of calcium influx were measured by Fluoro-Scan (Thermo Fisher Scientific Inc, Waltham, MA, USA). The excitation wavelength was 353 and 373 nm, and the emission wavelength was 510 nm. Non-selective nAChR antagonist, D-tubocurarine, was obtained from Sigma (St. Louis, MO, USA). In some experiments, MPDL22 cells were pretreated with 10⁻⁴ M D-tubocurarine, which was the most effective concentration for inhibiting nicotine-induced calcium influx in preliminary experiment, for 30 min before calcium measurement.

Mineralization assay

Histochemistry for staining calcified nodules was performed using the alizarin red staining method (Dahl, 1952). Cell layers were washed twice with PBS and then fixed in dehydrated ethanol. After fixation, the cell layers were stained with 1% alizarin red S in 0.1% NH₄OH (pH 6.3–6.5) for 5 min. The dishes were washed with H₂O and then observed microscopically, digitized and analyzed using the WinRoof software program (Mitani Corporation, Fukui, Japan).

Statistical analysis

Results were analyzed for statistical significance using the Student's *t*-test. Differences were considered significant at *P* values < 0.05.

Results

Expression of nAChRs mRNA and calcium signaling of nAChR in MPDL22 cells

To determine whether nAChRs were expressed in MPDL cells, mRNA was extracted from MPDL22 cells and analyzed by RT-PCR using mouse nAChR-specific primers. As shown in Figure 1a, MPDL22 cells were positive for α 3, α 4, α 7 and β 2 nAChR mRNA. To investigate whether the nAChRs expressed were functional, we analyzed cytosolic Ca²⁺ levels using Fluo-3AM. When nicotine was used as the agonist for nAChR, it elicited cytosolic Ca²⁺. Pretreatment with non-selective nAChR antagonist, D-tubocurarine, reduced nicotine-induced calcium mobilization (Figure 1b).

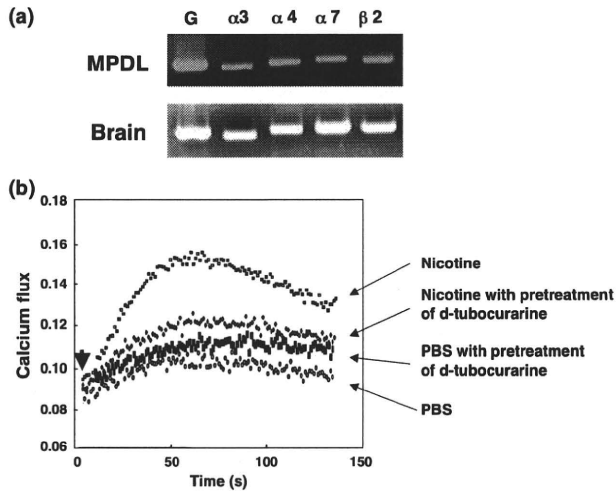


Figure 1 MPDL22 cells express functional nAChRs. (a) Expression of nAChR mRNA in MPDL22 cells was examined by RT-PCR. The number of PCR cycles was 33 and 24 for nAChRs and GAPDH, respectively. G: GAPDH. (b) Effects of nicotine on calcium mobilization in MPDL22 cells were monitored by measuring the fluorescence ratio (F340/380). Cells were pretreated for 30 min in the presence or absence of non-selective nAChR antagonist, D-tubocurarine (10^{-4} M), before addition of nicotine (10^{-3} M) or PBS. The arrowhead indicates the time of application of the stimulators. The results of one representative experiment from three identical experiments are shown

Effects of nicotine on MPDL22 proliferation

To investigate the effects of nicotine on the proliferation response of MPDL cells, cells were cultured for 48 h in a medium containing 1% FCS with or without nicotine. As previous studies revealed that FGF-2 induced the proliferation of PDL (Takayama *et al*, 1997), FGF-2 concentration of 100 ng ml^{-1} , which was the most optimal concentration for MPDL proliferation in preliminary experiment, was used as a positive control of this assay. The exposure of 10^{-8} M to 10^{-3} M nicotine did not induce significant proliferative responses in MPDL22 cells (Figure 2).

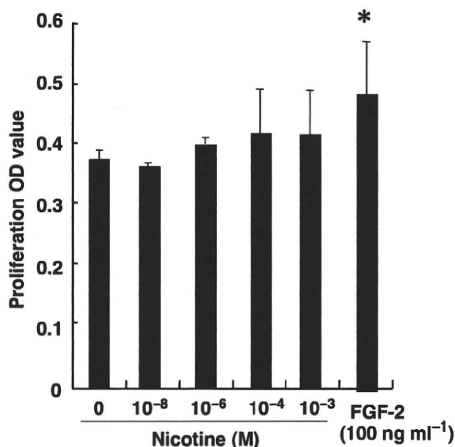


Figure 2 Effects of nicotine on proliferation of MPDL cells. MPDL cells were cultured with various doses of nicotine or FGF-2 (100 ng ml^{-1}) for 2 days. Values are means \pm s.d. of four determinations. * $P < 0.05$ compared with medium only

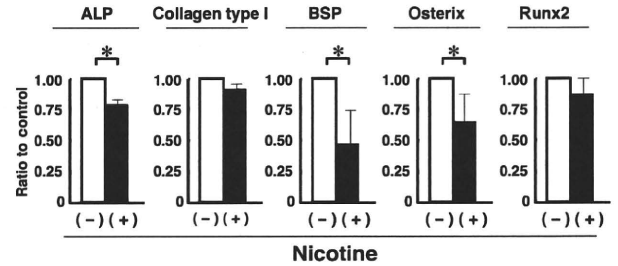


Figure 3 Analysis of mRNA expression of ECM in MPDL cells by RT-PCR. RNA samples were obtained from MPDL cells 2 days after nicotine treatment (10^{-3} M). The relative expression of each gene was standardized against the amount in HPRT as control and the expression of ECM in MPDL cells without nicotine was taken as 1.0. Values are means \pm s.d. of three or four determinations. * $P < 0.05$ compared with non-treated

Effects of nicotine on mRNA expression of ALP, BSP and osterix in MPDL22 cells

We then examined the effects of nicotine (10^{-3} M) on gene expression of the extracellular matrix (ECM) and osteoblastic transcription factors (Figure 3). MPDL22 cells, which were treated with nicotine, showed significantly decreased mRNA expression of ALP, BSP and osterix. In addition, the expression of collagen type I and *runx2* were also decreased compared with the control, but not significantly.

Effects of nicotine on mineralized nodule formation in MPDL22 cells

We cultured MPDL22 cells with or without nicotine in mineralization medium and then examined mineralized nodule formation on day 12. As shown in Figure 4a,b, nicotine reduced alizarin red staining intensity. Even a low concentration of nicotine (10^{-8} M) decreased mineralized nodule formation by the MPDL22 cells. Inhibitory effects of nicotine on the mineralization were partly abrogated by pretreatment with D-tubocurarine (Figure 4c). Next, we examined the time dependency of period of nicotine treatment on the inhibition of mineralization of MPDL cells (Figure 5). As shown in Figure 4, treatment with 10^{-3} M nicotine inhibited mineralization of MPDL22 cells. Interestingly, treatment with the same concentration of nicotine only for the first 8 days still considerably inhibited the mineralization. Similarly, nicotine treatment for both first 4 days (sample ID 4: day 0–4) and for the following 4 days (sample ID 5: day 4–8) still inhibited the mineralized nodule formation significantly.

Discussion

Little is known about the expression of nAChR subunits in hard tissue-forming cells. We previously reported that human dental pulp cells express nAChRs (Yanagita *et al*, 2008). In addition, $\alpha 4$ nAChR was expressed in human primary osteoblasts (Walker *et al*, 2001) and a recent study has reported human growth plate chondrocytes express $\alpha 5$, $\alpha 7$, $\beta 1$ and ϵ nAChR subunits (Kawakita *et al*, 2008). In this study, we found that

Figure 4 Effects of nicotine on mineralization of MPDL cells. (a) Effects of nicotine (10^{-8} M to 10^{-3} M) on mineralization in MPDL cells were examined by alizarin red staining. Alizarin red staining was performed after 12 days of culture in mineralization medium. Results of one representative experiment out of three identical experiments are shown. (b) The relative expression value of alizarin staining is shown in (a) and was quantitated and normalized to alizarin staining without nicotine. (c) Effects of D-tubocurarine on nicotine-dependent inhibition of the mineralization was examined. Alizarin red staining was performed after 12 days of culture in mineralization medium with nicotine (10^{-3} M) in the presence or absence of D-tubocurarine (10^{-4} M). Results of one representative experiment out of three identical experiments are shown. * $P < 0.05$ compared with medium only

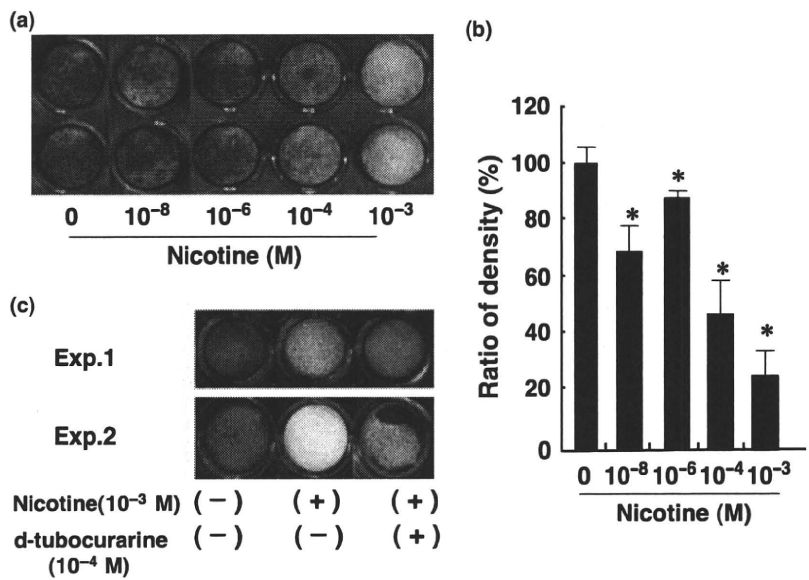
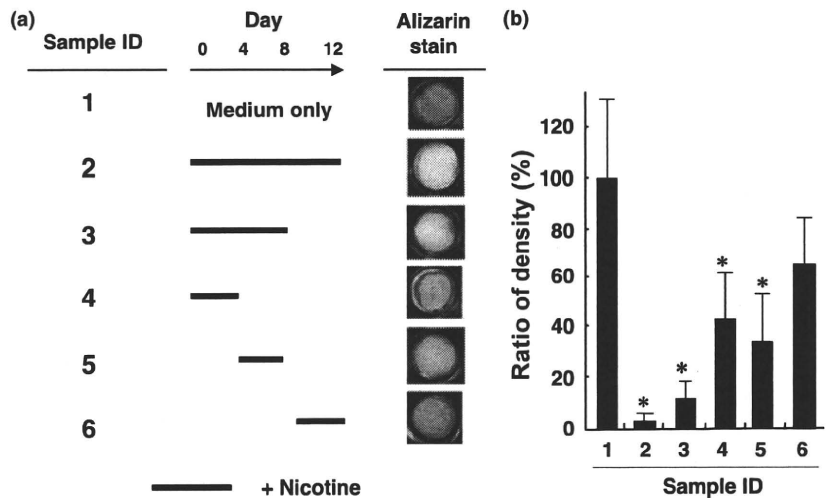


Figure 5 Effect of nicotine at differential stages of mineralization of MPDL cells. (a) Nicotine (10^{-3} M) was added to mineralization medium for the indicated periods and alizarin red staining was performed after 12 days of culture. (b) The relative expression value of the alizarin staining is shown in (a) and was quantitated and normalized to alizarin staining without nicotine. Results of one representative experiment out of two identical experiments are shown. * $P < 0.05$ compared with medium only



expression of $\alpha 3$, $\alpha 4$, $\alpha 7$ and $\beta 2$ nAChR subunits at mRNA level, which are reportedly the most abundantly expressed subtypes in murine brain and ganglion cells (Gahring and Rogers, 2005; Gotti *et al*, 2006) are detected in MPDL cells by RT-PCR. Unfortunately, we did not reveal the nAChR subunit expression at protein level in this study, and the detection of nAChR subunit proteins by immunoblot or immunohistochemistry remained to be the future work. Furthermore, nicotine elicited a transient calcium influx and D-tubocurarine, a non-selective nAChR antagonist, inhibited the calcium signals. This suggests that the effects of smoking on MPDL cells can be mediated via nAChR.

The results of this study show that nicotine did not change the proliferative responses of MPDL cells. In contrast, it was reported that nicotine has cytotoxicity and inhibits proliferation of human gingival fibroblasts and periodontal ligament cells (Giannopoulou *et al*, 2001; Chang *et al*, 2002). On the contrary, a

recent study showed that nicotine increased the proliferation rate of a murine preosteoblastic cell line, MC3T3-E1 (Sato *et al*, 2008). In addition, our previous study revealed that nicotine increased the DNA amounts in human dental pulp cells (Yanagita *et al*, 2008). Thus, the effect of nicotine on cellular proliferation is still controversial and may be cell-type dependent.

We examined the expression of some osteogenic markers, and revealed by RT-PCR that nicotine reduced the mRNA expression of ALP, BSP, and osterix (Figure 3). ALP is an enzyme marker of osteoblasts and participates in bone mineralization (Majeska and Wuthier, 1975). BSP is a small integrin-binding ligand N-linked glycoprotein, involved in the regulation of mineralization (Moses *et al*, 2006). Osterix, the osteoblast-specific transcription factor, has been identified as a modulator of bone formation and osteoblast differentiation (Nakashima and de Crombrughe, 2003). Thus,

the inhibitory effects of nicotine on the above-mentioned mRNA expression are correlate with that on the mineralization of MPDL22 cells. On the contrary, nicotine-induced BSP and collagen type I mRNA expression but down-regulated osteopontin mRNA in a human osteosarcoma cell line (Tanaka *et al*, 2005). Another study documented that 24-h treatment of nicotine up-regulated collagen type I, ALP and osteocalcin in osteosarcoma cells, but after 48 or 72-h incubation mRNA expression of these three genes was downregulated by nicotine in a dose-dependent manner (Rothem *et al*, 2009). In the case of chondrocytes, nicotine decreased the expression of ALP (Kawakita *et al*, 2008). Thus, the effects of nicotine on the mRNA expression of bone-related ECM also appears to be cell-type dependent.

Alizarin red staining showed that mineralization of MPDL22 cells was inhibited by nicotine (Figure 4a,b), and the inhibition was partly abrogated by D-tubocurarine, a non-selective nAChRs antagonist (Figure 4c). Furthermore, nicotine treatment for the first and second 4 days (sample ID 4, 5: day 0–4, 4–8) inhibited the mineralization. This result suggests that the suppressive effect of nicotine on the cytodifferentiation and mineralization of MPDL22 cells is culture-phase dependent. The fact that nicotine treatment for the last 4 days (sample ID 6: day 8–12) did not reduce the mineralization may suggest that MPDL22 should be committed to terminally differentiate at day 8. As shown in Figure 1b, D-tubocurarine almost completely inhibited nicotine-induced calcium influx, although suppression of mineralization was not completely recovered by the reagent (Figure 4c). In the case of calcium influx experiment, the incubation time was quite short, whereas cells were cultured for 12 days in mineralization assay. It is difficult at this point to establish a correlation between the initial, transient calcium signals and the mineralization results done on day 12. Measurement of calcium levels in the cells at day 12 may need to be done to accurately determine if early, transient calcium signals are linked to mineralization via an unknown signaling cascade.

Recently nicotine has been reported to induce p53 in osteoblasts (Sato *et al*, 2008). p53 is originally identified as a tumor suppressor, and promotes cell cycle arrest (Vogelstein *et al*, 2000). Interestingly it has been demonstrated that p53 regulates osteogenic differentiation (Wang *et al*, 2006). This suggests that p53 may be involved in the nicotine-induced inhibition of the differentiation of MPDL cells. Further studies are required to clarify the nicotine-induced signal cascade through nAChRs that influences the mineralization.

The association between smoking and progression of periodontal diseases, including alveolar bone loss, has been well-investigated (Grossi *et al*, 1994; Grossi *et al*, 1995; Ryder, 2007). Nicotine alters the cellular functions of PDL cells and gingival fibroblasts *in vitro* (Chang *et al*, 2002). Smokers demonstrate impaired periodontal tissue regeneration compared with non-smokers (Stavropoulos *et al*, 2004). The inhibitory

effect of nicotine on the mineralization of PDL cells partly accounts for the reason. Furthermore, smokers have been reported to suffer decrease of bone mass, increased risk of fracture and prolonged fracture repair (Krall and Dawson-Hughes, 1991, 1999). The important information is that the nicotine concentration in smokers' sera was 25–444 nM (Russell *et al*, 1980) and that serum nicotine levels of non-smokers exposed to secondhand smoke was around nM (5.9 ng ml⁻¹) (Pacifi *et al*, 1995). Figure 4a showed that a low concentration of nicotine circulating in the blood stream (~10 nM) can negatively influence the mineralization of PDL cells. These results suggest the possibility that secondhand smoke could be detrimental to periodontal health. In addition, inflammatory cytokines are detected in inflamed periodontal lesions, and some of those cytokines such as IL-1 β affect ECM expression (Chien *et al*, 1999). Therefore, to investigate the effect of nicotine on cytokine-induced ECM expression should be carried out in the future.

In conclusion, we have shown that nicotine is a potent negative regulator of cytodifferentiation and mineralization in PDL cells. Our studies suggest that nicotine causes progressing periodontal diseases and unfavorable prognoses after periodontal treatments.

Acknowledgements

This work was supported in part by Grants-in-Aid for Scientific Research (No. 2039529, 20390530, 20592427) and the 21st Century COE entitled 'Origination of Frontier BioDentistry' at Osaka University Graduate School of Dentistry supported by the Ministry of Education, Culture, Sports, Science and Technology.

Competing interests

None declared.

Ethical approval

Not required.

References

- Chang YC, Huang FM, Tai KW, Yang LC, Chou MY (2002). Mechanisms of cytotoxicity of nicotine in human periodontal ligament fibroblast cultures *in vitro*. *J Periodontol Res* **37**: 279–285.
- Chien HH, Lin WL, Cho MI (1999). Interleukin-1 β -induced release of matrix proteins into culture media causes inhibition of mineralization of nodules formed by periodontal ligament cells *in vitro*. *Calcif Tissue Int* **64**: 402–413.
- Dahl LK (1952). A simple and sensitive histochemical method for calcium. *Proc Soc Exp Biol Med* **80**: 474–479.
- Feyerabend C, Higenbottam T, Russell MA (1982). Nicotine concentrations in urine and saliva of smokers and non-smokers. *Br Med J (Clin Res Ed)* **284**: 1002–1004.
- Gahring LC, Rogers SW (2005). Neuronal nicotinic acetylcholine receptor expression and function on nonneuronal cells. *AAPS J* **7**: E885–E894.
- Giannopoulou C, Roehrich N, Mombelli A (2001). Effect of nicotine-treated epithelial cells on the proliferation and

- collagen production of gingival fibroblasts. *J Clin Periodontol* **28**: 769–775.
- Gotti C, Zoli M, Clementi F (2006). Brain nicotinic acetylcholine receptors: native subtypes and their relevance. *Trends Pharmacol Sci* **27**: 482–491.
- Grossi SG, Zambon JJ, Ho AW, Koch G, Dunford RG, Machtei EE, Norderyd OM, Genco RJ (1994). Assessment of risk for periodontal disease. I. Risk indicators for attachment loss. *J Periodontol* **65**: 260–267.
- Grossi SG, Genco RJ, Machtei EE, et al. (1995). Assessment of risk for periodontal disease. II. Risk indicators for alveolar bone loss. *J Periodontol* **66**: 23–29.
- Hoffmann D, Adams JD (1981). Carcinogenic tobacco-specific N-nitrosamines in snuff and in the saliva of snuff dippers. *Cancer Res* **41**: 4305–4308.
- Kageyama-Yahara N, Suehiro Y, Yamamoto T, Kadowaki M (2008). IgE-induced degranulation of mucosal mast cells is negatively regulated via nicotinic acetylcholine receptors. *Biochem Biophys Res Commun* **377**: 321–325.
- Kawakita A, Sato K, Makino H, et al. (2008). Nicotine acts on growth plate chondrocytes to delay skeletal growth through the alpha7 neuronal nicotinic acetylcholine receptor. *PLoS One* **3**: e3945.
- Krall EA, Dawson-Hughes B (1991). Smoking and bone loss among postmenopausal women. *J Bone Miner Res* **6**: 331–338.
- Krall EA, Dawson-Hughes B (1999). Smoking increases bone loss and decreases intestinal calcium absorption. *J Bone Miner Res* **14**: 215–120.
- Lofroth G (1989). Environmental tobacco smoke: overview of chemical composition and genotoxic components. *Mutat Res* **222**: 73–80.
- Majeska RJ, Wuthier RE (1975). Studies on matrix vesicles isolated from chick epiphyseal cartilage. Association of pyrophosphatase and ATPase activities with alkaline phosphatase. *Biochim Biophys Acta* **391**: 51–60.
- Martinez-Canut P, Guarinos J, Bagan JV (1996). Periodontal disease in HIV seropositive patients and its relation to lymphocyte subsets. *J Periodontol* **67**: 33–36.
- Moses KD, Butler WT, Qin C (2006). Immunohistochemical study of small integrin-binding ligand, N-linked glycoproteins in reactionary dentin of rat molars at different ages. *Eur J Oral Sci* **114**: 216–222.
- Nakashima K, de Crombrughe B (2003). Transcriptional mechanisms in osteoblast differentiation and bone formation. *Trends Genet* **19**: 458–466.
- Pacifici R, Altieri I, Gandini L, et al. (1995). Environmental tobacco smoke: nicotine and cotinine concentration in semen. *Environ Res* **68**: 69–72.
- Rothem DE, Rothem L, Soudry M, Dahan A, Eliakim R (2009). Nicotine modulates bone metabolism-associated gene expression in osteoblast cells. *J Bone Miner Metab* **27**: 555–561.
- Russell MA, Jarvis M, Iyer R, Feyerabend C (1980). Relation of nicotine yield of cigarettes to blood nicotine concentrations in smokers. *Br Med J* **280**: 972–976.
- Ryder MI (2007). The influence of smoking on host responses in periodontal infections. *Periodontol* **43**: 267–277.
- Sato T, Abe T, Nakamoto N, et al. (2008). Nicotine induces cell proliferation in association with cyclin D1 up-regulation and inhibits cell differentiation in association with p53 regulation in a murine pre-osteoblastic cell line. *Biochem Biophys Res Commun* **377**: 126–130.
- Seo BM, Miura M, Gronthos S, et al. (2004). Investigation of multipotent postnatal stem cells from human periodontal ligament. *Lancet* **364**: 149–155.
- Seow WK, Thong YH, Nelson RD, MacFarlane GD, Herzberg MC (1994). Nicotine-induced release of elastase and eicosanoids by human neutrophils. *Inflammation* **18**: 119–127.
- Stavropoulos A, Mardas N, Herrero F, Karring T (2004). Smoking affects the outcome of guided tissue regeneration with bioresorbable membranes: a retrospective analysis of intrabony defects. *J Clin Periodontol* **31**: 945–950.
- Takayama S, Murakami S, Miki Y, et al. (1997). Effects of basic fibroblast growth factor on human periodontal ligament cells. *J Periodontol Res* **32**: 667–675.
- Tanaka H, Tanabe N, Suzuki N, et al. (2005). Nicotine affects mineralized nodule formation by the human osteosarcoma cell line Saos-2. *Life Sci* **77**: 2273–2284.
- Vogelstein B, Lane D, Levine AJ (2000). Surfing the p53 network. *Nature* **408**: 307–310.
- Walker LM, Preston MR, Magnay JL, Thomas PB, El Haj AJ (2001). Nicotinic regulation of c-fos and osteopontin expression in human-derived osteoblast-like cells and human trabecular bone organ culture. *Bone* **28**: 603–608.
- Wang X, Kua HY, Hu Y, et al. (2006). p53 functions as a negative regulator of osteoblastogenesis, osteoblast-dependent osteoclastogenesis, and bone remodeling. *J Cell Biol* **172**: 115–125.
- Yamada S, Tomoeda M, Ozawa Y, et al. (2007). PLAP-1/aspurin: a novel negative regulator of periodontal ligament mineralization. *J Biol Chem* **282**: 23070–23080.
- Yanagita M, Kashiwagi Y, Kobayashi R, Tomoeda M, Shimabukuro Y, Murakami S (2008). Nicotine inhibits mineralization of human dental pulp cells. *J Endod* **34**: 1061–1065.

Role of Mechanical Stress-induced Glutamate Signaling-associated Molecules in Cytodifferentiation of Periodontal Ligament Cells^{*S}

Received for publication, December 20, 2009, and in revised form, June 23, 2010. Published, JBC Papers in Press, June 24, 2010, DOI 10.1074/jbc.M109.097303

Chiharu Fujihara^{†1}, Satoru Yamada^{†1}, Nobuhiro Ozaki[†], Nobuo Takeshita[§], Harumi Kawaki[§], Teruko Takano-Yamamoto[§], and Shinya Murakami^{†2}

From the [†]Department of Periodontology, Division of Oral Biology and Disease Control, Osaka University Graduate School of Dentistry, 1-8 Yamadaoka, Suita, Osaka 565-0871, Japan and the [§]Division of Orthodontics and Dentofacial Orthopedics, Department of Oral Health and Development Sciences, Tohoku University Graduate School of Dentistry, 4-1 Seiryō-machi, Aoba-ku, Sendai 980-8578, Japan

In this study, we analyzed the effects of tensile mechanical stress on the gene expression profile of *in vitro*-maintained human periodontal ligament (PDL) cells. A DNA chip analysis identified 17 up-regulated genes in human PDL cells under the mechanical stress, including *HOMER1* (homer homolog 1) and *GRIN3A* (glutamate receptor ionotropic *N*-methyl-D-aspartate 3A), which are related to glutamate signaling. RT-PCR and real-time PCR analyses revealed that human PDL cells constitutively expressed glutamate signaling-associated genes and that mechanical stress increased the expression of these mRNAs, leading to release of glutamate from human PDL cells and intracellular glutamate signal transduction. Interestingly, exogenous glutamate increased the mRNAs of cytodifferentiation and mineralization-related genes as well as the ALP (alkaline phosphatase) activities during the cytodifferentiation of the PDL cells. On the other hand, the glutamate signaling inhibitors riluzole and (+)-MK801 maleate suppressed the alkaline phosphatase activities and mineralized nodule formation during the cytodifferentiation and mineralization. Riluzole inhibited the mechanical stress-induced glutamate signaling-associated gene expressions in human PDL cells. Moreover, *in situ* hybridization analyses showed up-regulation of glutamate signaling-associated gene expressions at tension sites in the PDL under orthodontic tooth movement in a mouse model. The present data demonstrate that the glutamate signaling induced by mechanical stress positively regulates the cytodifferentiation and mineralization of PDL cells.

The ability of cells to sense and respond to physical stress is required for tissue homeostasis and normal development. In muscle, bone, tendon, periodontium, and the cardiovascular system, applied forces of physiological magnitude regulate cellular processes that are critical for normal tissue and organ functions, such as differentiation, proliferation, and migration

(1). The periodontal ligament (PDL)³ is a connective tissue interposed between the roots of teeth and the inner wall of the tooth-supporting bone (alveolar bone) socket. The PDL constitutively and iatrogenically receives mechanical stress, such as occlusal pressure and orthodontic forces, which have effects on the homeostasis of the PDL (2). Proper mechanical stress on teeth induces not only the proliferation and differentiation of PDL cells into osteoblasts and cementoblasts but also the synthesis and degradation of extracellular matrix (ECM) molecules (3). For example, during orthodontic tooth movement, two types of sites (tension sites and pressure sites) arise around the tooth through the orthodontic force. At the tension sites, the PDL is stretched, and the expressions of bone-related genes, such as osteocalcin (4) and bone sialoprotein (5), are up-regulated, such that bone formation is finally induced on the alveolar bone facing the tooth root (6). On the other hand, at the pressure sites, the PDL is compressed, and osteoclasts are activated. Consequently, resorption of the alveolar bone is induced. An orchestrated balance between bone formation and resorption controls tooth movement (7). In contrast, elimination of mechanical stress on teeth is known to cause atrophy of the PDL *in vivo* (8). Kaneko *et al.* (9) reported that loss of occlusal function by extraction of the antagonistic upper molars of rats caused atrophic changes in the PDL of the lower molars, such as narrowing of the space, disorientation of collagen fibers, and decreases in proteoglycans. These findings indicate that mechanical stress on teeth affects the remodeling of the PDL, cementum, and alveolar bone. Thus, it is important to clarify the physiological functions of mechanical stress on the PDL.

To clarify the molecular basis of the mechanical stress-regulated PDL functions, we analyzed the gene expression profile of human PDL cells receiving tensile mechanical stress *in vitro*. Interestingly, an oligo-DNA chip analysis identified two glutamate signaling-associated genes, *HOMER1* (homer homolog 1) and *GRIN3A* (glutamate receptor ionotropic *N*-methyl-D-aspartate 3A), among the up-regulated genes. L-Glutamate is the most abundant amino acid in the central nervous system and plays important roles in neurotransmission (10). Stimulation of

^{*} This work was supported by Grants-in-aid 20390529 and 20390530 from the Japan Society for the Promotion of Science and Research Grant H21-001 from the Ministry of Health, Labor, and Welfare.

^S The on-line version of this article (available at <http://www.jbc.org>) contains supplemental Tables 1 and 2.

[†] These authors contributed equally to this work.

² To whom correspondence should be addressed. Tel.: 81-6-6879-2930; Fax: 81-6-6879-2934; E-mail: ipshinya@dent.osaka-u.ac.jp.

³ The abbreviations used are: PDL, periodontal ligament; MK801, (+)-MK801 maleate; CREB, cAMP-response element-binding protein; ECM, extracellular matrix; Ca²⁺, calcium ion; NMDAR, *N*-methyl-D-aspartate receptor; IP₃, inositol 1,4,5-trisphosphate; aRNA, amino allyl RNA; DIG, digoxigenin.

Mechanical Stress-induced Glutamate Signaling in PDL Cells

presynaptic cells promotes the release of glutamate, and the released glutamate induces glutamate signaling by binding to glutamate receptors on the postsynaptic cells. In addition to the central nervous system, glutamate signaling has been observed in non-neural tissues, such as the taste buds (11), spleen (12), and bone (13), and modulates various functions of each tissue (14). However, involvement of glutamate signaling in the PDL has not been reported. In the present study, we further analyzed the gene expression and functions of glutamate signaling-associated molecules in PDL cells to elucidate the roles of glutamate signaling in the PDL.

EXPERIMENTAL PROCEDURES

Reagents— α -Modified Eagle's medium was obtained from Nikken Biomedical Laboratory (Kyoto, Japan). Fetal calf serum (FCS) was purchased from JRH Biosciences (Lenexa, KS). Riluzole, bisbenzimidazole (Hoechst 33258), and DNA sodium salt (from calf thymus) were products from Sigma. Kanamycin, L-glutamate, β -glycerophosphate, ascorbic acid, and *p*-nitrophenyl phosphate were obtained from Wako Pure Chemical Industries (Osaka, Japan). (+)-MK801 maleate (MK801) was purchased from Tocris Cookson (Bristol, UK).

Cell Culture—Human PDL cells were isolated as described previously (15). The cells were cultured in α -modified Eagle's medium supplemented with 10% FCS, 50 units/ml penicillin G, and 50 μ g/ml streptomycin at 37 °C under 5% CO₂. For the induction of cytodifferentiation, human PDL cells were cultured in α -modified Eagle's medium with 10% FCS in the presence of 10 mM β -glycerophosphate and 50 μ g/ml ascorbic acid (mineralization-inducing medium). The mineralization-inducing medium was replaced every 3 days.

Application of Mechanical Stress—To allow cell attachment, 10-cm² silicon membrane chambers (Scholertec, Osaka, Japan) were coated with 0.3 mg/ml pepsin-digested collagen type I derived from swine (Nitta Gelatin, Osaka, Japan) according to the Scholertec manufacturer's instructions. Human PDL cells were transferred to the chambers at a density of 1.5×10^4 cell/cm² and cultured in α -modified Eagle's medium with 10% FCS for 3 days. The chambers were applied to a stretch apparatus, Scholertec NS-350 (Scholertec), and the cells were repeatedly stretched and relaxed at 37 °C under 5% CO₂ *in vitro*. The force conditions were 0.5 Hz (30 cycles/min) with 110% elongation for 0, 24, and 48 h. This force represented the physiological conditions of occlusal force (16). Cells seeded on the chambers without stretching served as controls.

Oligo-DNA Chip Analysis—Total RNA (1 μ g) extracted from the stretched human PDL cells using RNA Bee (Tel-Test Inc., Friendswood, TX) was targeted to synthesize experimental amino allyl RNA (aRNA) using an Amino Allyl MessageAmp aRNA kit (Ambion Inc., Austin, TX) according to the manufacturer's protocol. Cy3 or Cy5 fluorescent dyes (Amersham Biosciences) were incorporated into the aRNAs by an indirect labeling method. The labeled aRNAs were fragmented and hybridized to an AceGene Human Oligo Chip 30K (Hitachi Software Engineering Co., Ibaraki, Japan) consisting of 30,000 human oligonucleotide features. After a 12-h hybridization, the DNA chip was washed according to the manufacturer's instructions, and the fluorescence intensities were scanned with a Scan

Array Lite (PerkinElmer Life Sciences). The resulting image was analyzed using Scan Array Express version 2.0. Normalization using LOWELL was performed for data obtained from the raw data.

Real-time RT-PCR Analysis—cDNA was synthesized from the purified total RNA using a high capacity cDNA reverse transcription kit (Applied Biosystems, Carlsbad, CA) according to the manufacturer's instructions. The obtained cDNA was mixed with Power PCR SYBR Master Mix (Applied Biosystems) and gene-specific primers (Takara Bio, Shiga, Japan). The sequences of the primers are shown in supplemental Table 1. Real-time PCR was performed using a 7300 fast real-time RT-PCR system (Applied Biosystems) according to the manufacturer's instructions. The amplification conditions consisted of an initial 15-min denaturation step at 95 °C, followed by 40 cycles of denaturation at 94 °C for 15 s, annealing at 60 °C for 30 s, and elongation at 72 °C for 30 s. The dissociation curves were analyzed to ensure the amplification of a single PCR product. Three independent assays were performed for each primer. The amount of cDNA was calculated for each sample from the standard curve. The relative expression is shown after normalization by the gene expression of *HPRT* (hypoxanthine phosphoribosyltransferase).

Conventional RT-PCR Analysis—The purified total RNA was reverse-transcribed with SuperScript II reverse transcriptase (Invitrogen) and an oligo(dT) primer (Invitrogen). The synthesized cDNA was mixed with AmpliTaq Gold DNA polymerase (Applied Biosystems) and gene-specific primers synthesized by GeneDesign Inc. (Osaka, Japan). The sequences of the primers are shown in supplemental Table 2. PCR was performed using a PTC-200 Peltier thermal cycler (Bio-Rad). The amplification conditions consisted of an initial incubation at 94 °C for 9 min, followed by cycles of denaturation at 94 °C for 60 s, annealing at the temperatures indicated in supplemental Table 2, and elongation at 72 °C for 60 s. The PCR products were evaluated by agarose gel electrophoresis.

Determination of Released Glutamate—The levels of glutamate were determined by a modification of an enzyme-linked fluorimetric assay according to a previously published protocol (17). In the presence of glutamate dehydrogenase (Oriental Yeast Co., Osaka, Japan) and β -nicotinamide adenine dinucleotide phosphate (β -NADP⁺) (Oriental Yeast Co.), released glutamate is oxidized to α -ketoglutarate with the production of NADPH, which can be determined fluorometrically to quantify the glutamate concentration. Briefly, human PDL cells were grown in 6-well plates or stretched on chambers. The supernatants were collected from each well, filtered with a Minisart 0.2- μ m filter (Sartorius Stedim Biotech, Goettingen, Germany), and prewarmed to 25 °C with 7 mM β -NADP⁺ (pH 7.4). The reaction was initiated by the addition of glutamate dehydrogenase (9 IU/ml). After incubation for 15 min, the absorbance was measured at 320 nm using a GeneQuant pro "S" spectrophotometer (Amersham Biosciences) and compared with standard curves constructed using known concentrations of L-glutamate. The DNA concentrations in the cell layers were determined by subtracting the amount of glutamate in the medium as the absorbance of the background in advance.

Mechanical Stress-induced Glutamate Signaling in PDL Cells

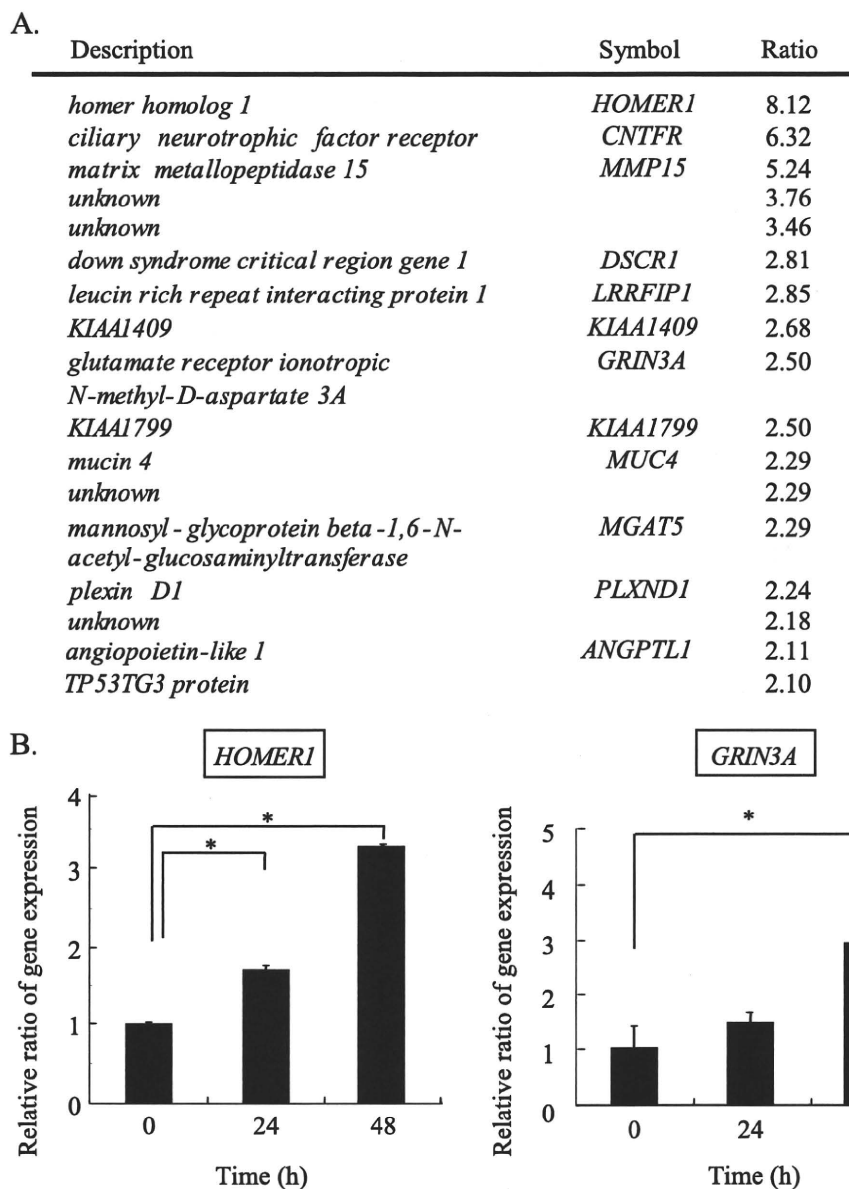


FIGURE 1. Gene expression profile of human PDL cells under mechanical stress. A, the oligo-DNA chip analysis revealed the gene expression profile of human PDL cells after the application of mechanical stress for 48 h. The ratios are the relative ratio of each gene expression in the 48-h stretched cells to that in the non-stretched cells. B, real-time RT-PCR was performed for the gene expressions of *HOMER1* and *GRIN3A* in human PDL cells after the application of mechanical stress for 0, 24, and 48 h. The expressions of *HOMER1* and *GRIN3A* were normalized by the expression of *HPRT*. The values are shown as the relative ratios to 0 h. Values represent the means \pm S.D. (error bars) of triplicate assays. Similar results were obtained in three separate experiments, and representative data are shown. *, $p < 0.05$, compared with 0 h.

Western Blotting Analysis of Phosphorylation of cAMP-response Element-binding Protein (CREB) in Human PDL Cells—Human PDL cells stimulated by glutamate or mechanical stress were lysed with cell lysis buffer (50 mM Tris-HCl, pH 7.4; 1% Nonidet P-40; 0.25% sodium deoxycholate; 150 mM NaCl; 1 mM EDTA; 1 mM PMSF; 1 mg/ml aprotinin, leupeptin, and pepstatin; 1 mM Na_3VO_4 ; 1 mM NaF; 1 μM microcystin). The protein concentrations of the cell lysates were measured using a BCA protein assay kit (Pierce) according to the manufacturer's instructions. The cell lysates were subjected to 7.5% SDS-PAGE and then electroblotted onto polyvinylidene difluoride membranes. A rabbit anti-phospho-CREB antibody (1:1000; Milli-

pore, Temecula, CA) and a rabbit anti-CREB antibody (1:1000, Millipore) were used as the primary antibodies. A horseradish peroxidase-linked goat anti-rabbit IgG antibody (Cappel, Aurora, OH) was used as the secondary antibody. Immunoreactive proteins were detected using an ECL Plus kit (GE Healthcare).

Measurement of Intracellular Ca^{2+} Content—Fluorescence measurements of the intracellular Ca^{2+} contents were performed using a Fluoskan Ascent FC spectrophotometer (Thermo Fisher Scientific Inc., Waltham, MA) and a Calcium Kit-Fluo 3 (Dojindo Laboratories, Kumamoto, Japan) according to the manufacturers' protocols. Briefly, human PDL cells were seeded at a density of 1.5×10^4 cells/well on a black 96-well plate. After incubation for 24 h, the cells were washed with PBS and incubated in loading buffer containing Fluo 3-AM for 1 h. The cells were washed with PBS, and then 100 μl of recording medium containing 0.04% Pluronic F-127 and 1.25 mM probenecid was added to each well. The PDL cells were then stimulated with 20 μl of L-glutamate (600 μM). The fluorescence intensities were immediately measured at 1-s intervals using wavelengths of 485 nm for excitation and 538 nm for emission.

Cell Survival Analysis—Human PDL cells were seeded on 12-well dishes at a density of 1.0×10^5 cells/well. After 24 h of serum starvation, the cells were cultured in the presence or absence of inhibitors at specified concentrations for 0, 24, and 48 h. The cells were then treated with trypsin for 5 min at 37 $^\circ\text{C}$ and

centrifuged at $1,200 \times g$ for 5 min. The cell pellets were resuspended with PBS. The live and dead cells were manually counted with a hemocytometer after 0.5% trypan blue staining.

Determination of ALP (Alkaline Phosphatase) Activity—ALP activities were measured according to the procedure described by Bessey *et al.* (18). Briefly, human PDL cells were placed in 12-well plates at a density of 1.0×10^5 cells/well. After two washes with PBS, the cells were sonicated in 2 ml of distilled water at 4 $^\circ\text{C}$. Next, 500 μl of Tris-HCl (1.0 M, pH 9.0), 100 μl of MgCl_2 (5 mM), and 150 μl of Triton X-100 (0.04%) were mixed with 150 μl of the supernatants. The addition of 100 μl of *p*-nitrophenyl phosphate (5 mM) as a substrate was used to deter-

Mechanical Stress-induced Glutamate Signaling in PDL Cells

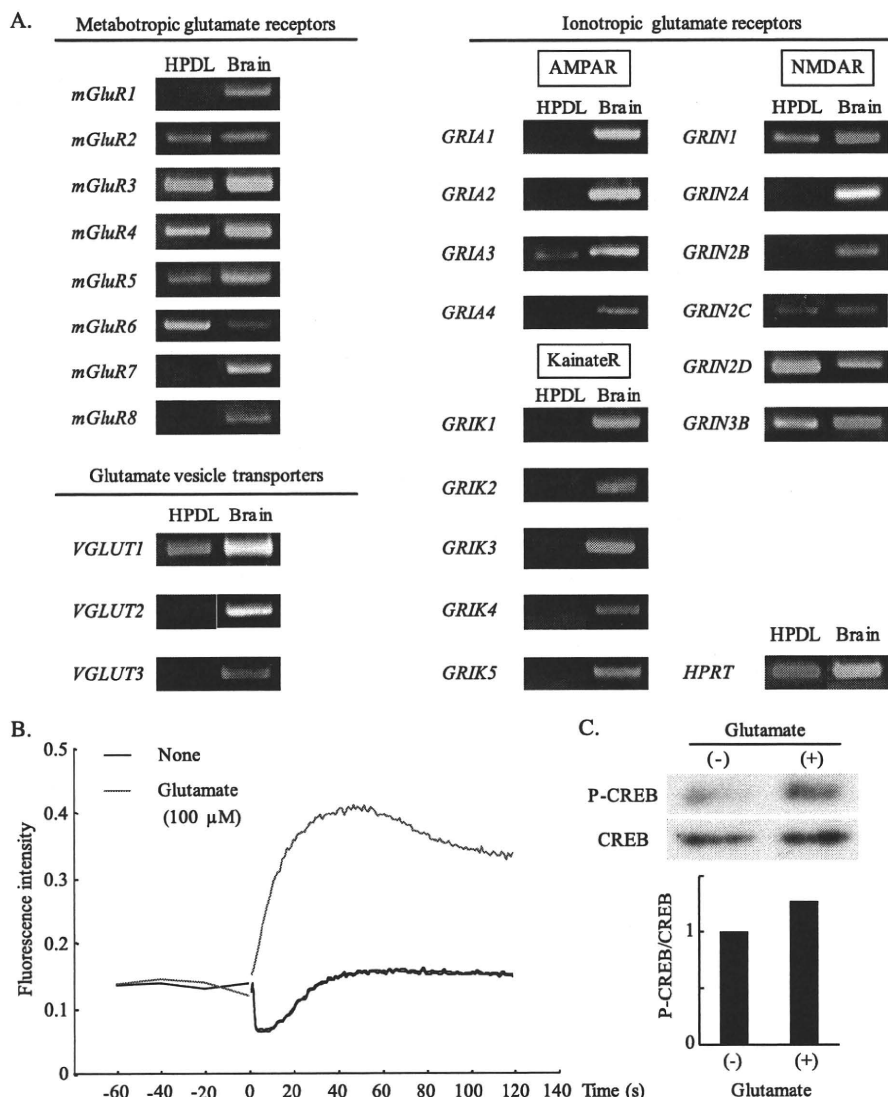


FIGURE 2. Gene expressions and functions of glutamate signaling-associated molecules in human PDL cells. *A*, human PDL cells were harvested for RNA isolation, followed by RT-PCR for the gene expressions of glutamate signaling-associated molecules. RNA derived from the human brain was used as a positive control. The numbers of PCR cycles were 40 for metabotropic glutamate receptors and 35 for ionotropic glutamate receptors and glutamate vesicle transporters. The number of PCR cycles was 30 for *HPRT*. Representative results of three independent experiments are shown. *B*, human PDL cells were labeled with the Ca^{2+} fluorescent agent Fluo 3-AM and stimulated with 100 μ M exogenous glutamate. The fluorescence intensity was measured to assess the intracellular Ca^{2+} influx. *Black line* (None), distilled water alone; *red* (Glutamate), glutamate (100 μ M). Representative results of four independent experiments are shown. *C*, human PDL cells were stimulated with glutamate (500 μ M) for 40 min and then lysed. The cell lysates were subjected to SDS-PAGE and transferred to a membrane that was simultaneously probed with antibodies against phospho-CREB (*P-CREB*) and CREB protein. A quantitative Western blotting analysis is shown as the ratios of the intensities of phospho-CREB and CREB. Representative results of three independent experiments are shown.

mine the ALP activities. The samples were incubated at 37 $^{\circ}$ C for 30 min, and 0.25 ml of 1 N NaOH was added to stop the reaction. The absorbance of each sample was measured at 405 nm using a microplate reader (model 680; Bio-Rad). One unit of activity was defined as the enzyme activity hydrolyzing 1 nmol of *p*-nitrophenyl phosphate in 30 min.

Determination of Cellular DNA Contents—The DNA content was measured by a modification of the method of Labarca and Paigen (19). Briefly, human PDL cells were washed twice with PBS and sonicated on ice in 2 ml of distilled water. Hoechst 33258 was prepared by dissolution in NaCl (2 M) plus Tris-HCl (25 mM, pH 7.5), and 25 μ l of the resulting Hoechst 33258 solu-

tion (5 μ g/ml) was added to 100 μ l of the supernatants. The fluorescence was monitored at an emission wavelength of 450 nm after excitation at 356 nm using a spectrophotometer (Fluoskan Ascent FC, Thermo Fisher Scientific Inc.). The concentration of DNA in the samples was determined by a standard curve based on various concentrations of calf thymus DNA.

Alizarin Red Staining—Histochemical staining of Ca^{2+} was performed by a modification of the method described by Dahl (20). Briefly, human PDL cell layers were washed twice with PBS and then fixed with dehydrated ethanol for 10 min. After fixation, the cell layers were stained with 1% alizarin red S (Wako Pure Chemical Industries) in 0.1% NH_4OH (pH 6.5) for 5 min. The wells were washed with distilled water and scanned with a GT-9700F system (Epson, Nagano, Japan). The density of calcified nodules in each well was calculated using the software Win ROOF version 5.6 (Mitani, Fukui, Japan).

Preparation of a Mouse Mechanical Stimulation Model by Experimental Tooth Movement and Tissue Preparation—The first molars of 6-week-old male ICR mice were moved according to the method described Sakai *et al.* (21). Briefly, a nickel-titanium wire, 0.012 inches in diameter, was fixed to the maxillary incisor with resin, and the right maxillary first molar was moved toward the palatal side for 3 days. The force loaded was directly measured on a plaster model before and after the placement of the wire in each mouse using a dial tension gauge (DTG-10NP, Mitutoyo (Kawasaki, Japan)).

A 10-g force was applied to the tooth at 0 h, and no further adjustment was necessary during the 3 days. The animals were anesthetized and perfused with 4% paraformaldehyde (pH 7.4). Samples of the alveolar bone region were prepared at 12 and 24 h after the initiation of experimental tooth movement and fixed in the above solution for \sim 24 h at 4 $^{\circ}$ C. The specimens were decalcified in 20% EDTA for 14 days at 4 $^{\circ}$ C, dehydrated, and embedded in paraffin. The resulting tissue blocks were cut into 7- μ m-thick cross-sections and mounted on triethoxyaminopropylsilane-coated slides. The experimental protocol was approved by the Animal Committee of Tohoku University.

Mechanical Stress-induced Glutamate Signaling in PDL Cells

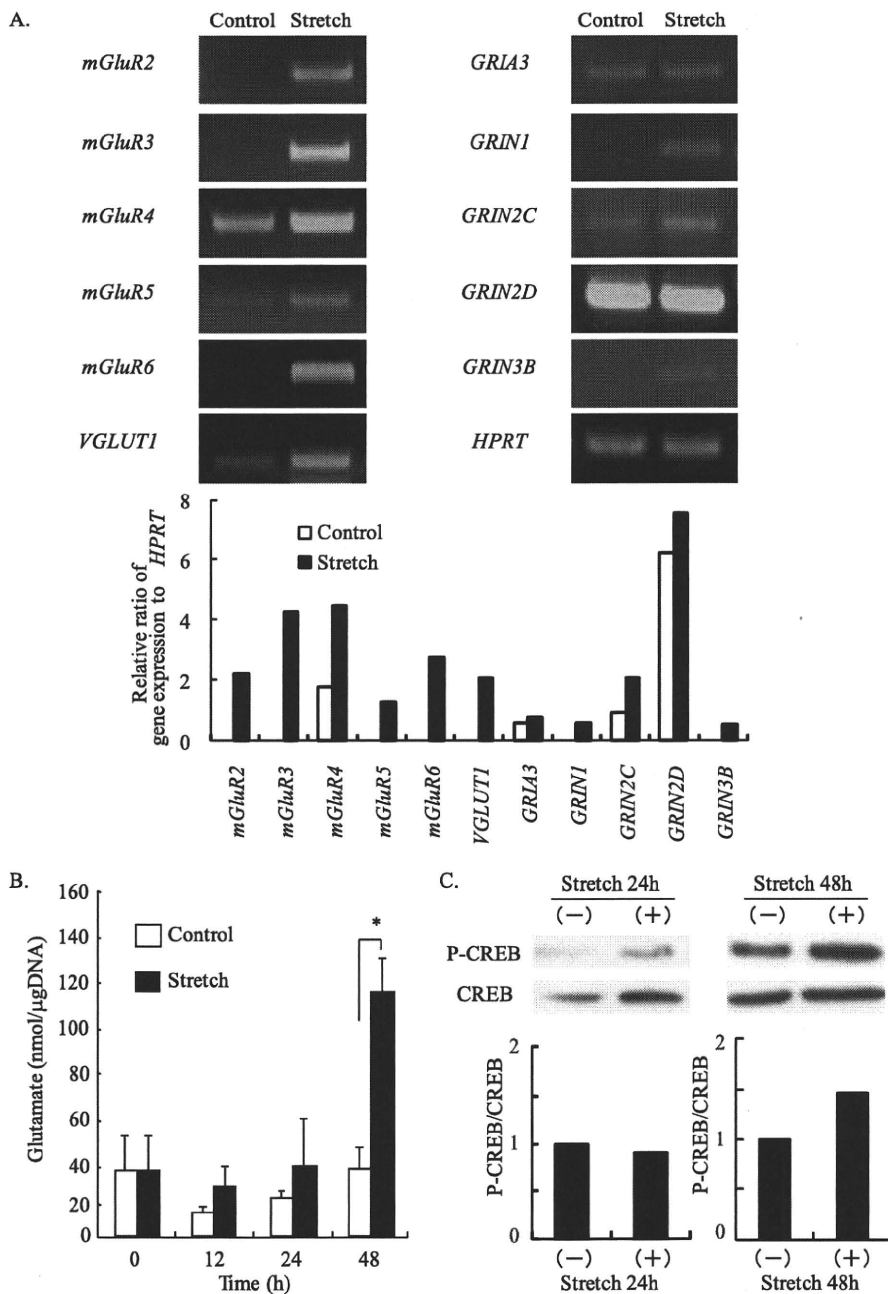


FIGURE 3. Effects of human PDL cells under mechanical stress on glutamate signaling. *A*, RT-PCR analyses were performed for the expressions of glutamate signaling-associated genes in human PDL cells after the application of mechanical stress for 24 h. The numbers of PCR cycles were 35 for *mGluR2-6* and *VGLUT1*, 30 for *GRIA3* and *HPRT*, 40 for *GRIN1* and *GRIN3B*, and 38 for *GRIN2C* and *GRIN2D*. A quantitative analysis of the PCR products using the software Win ROOF is shown as the ratio of the intensities of each gene expression and *HPRT*. *Control*, non-stretched human PDL cells; *Stretch*, stretched cells. Representative results of three independent experiments are shown. *B*, the release of glutamate was determined in supernatants from human PDL cells after the application of mechanical stress for the indicated times. Values are shown as the relative ratios to 0 h. Values represent the means \pm S.D. (error bars) of triplicate assays. Similar results were obtained in three separate experiments, and representative data are shown. *, $p < 0.05$, compared with non-stretched cells. *C*, Western blotting analysis was carried out for phospho-CREB (*P-CREB*) and CREB proteins in human PDL cells after the application of mechanical stress for the indicated times. A quantitative analysis is shown as the ratios of the intensities of phospho-CREB and CREB. Similar results were obtained in three separate experiments, and representative data are shown.

Probe Preparation—Commercial mouse *Homer1*, *Vglut1*, *Grin1* (glutamate receptor ionotropic *N*-methyl-D-aspartate 1), *mGluR3* (metabotropic G-protein-coupled receptor 3), *mGluR5*, and *mGluR6* full-length cDNA clones were purchased from Source BioScience Plc Geneservice (Cambridge, England). By

using these clones as templates for RT-PCR, we obtained the corresponding cDNA fragments. The DNA fragment for *Homer1* was 501 bp (site location from 388 to 888 bp of accession number NM_147176), that for *Vglut1* (vesicular glutamate transporter 1) was 364 bp (site location from 515 to 878 bp of accession number NM_182993), that for *Grin1* was 478 bp (site location from 1 to 477 bp of accession number NM_008169), that for *mGluR3* was 509 bp (site location from 202 to 710 bp of accession number NM_181850), that for *mGluR5* was 505 bp (site location from 98 to 602 bp of accession number NM_001081414), and that for *mGluR6* was 485 bp (site location from 58 to 542 bp of accession number NM_173372). The DNA fragment for mouse *Runx2* was 701 bp (site location from 3324 to 4024 bp of accession number NM_001146038), that for mouse osteocalcin was 403 bp (site location from 39 to 441 bp of accession number NM_007541), and that for mouse type I collagen was 241 bp (site location from 119 to 359 bp of accession number NM_007742). The fragments were subcloned into pGEM-T Easy vectors (Promega, Madison, WI) and used to generate sense and antisense probes. Digoxigenin (DIG)-11-UTP-labeled single-stranded RNA probes were prepared using a DIG RNA labeling kit (Roche Applied Science) according to the manufacturer's instructions.

In Situ Hybridization—*In situ* hybridization was performed as described previously (4), with minor modifications. Briefly, sections were deparaffinized and fixed with 4% paraformaldehyde for 20 min at room temperature. The sections were then washed and incubated with 5 μ g/ml proteinase K (Roche Applied Science) in 10 mM Tris-HCl (pH 8) and 1 mM EDTA for 15 min at room temperature. The sections were refixed, treated with 0.2 N HCl for 10 min at room temperature, washed again, and equilibrated with 0.1 M triethanolamine-HCl buffer (pH 8) for 2 min. Acetylation of the sections was performed by incubation with freshly prepared 0.25% acetic anhydride for 10 min at room temperature. The sections were dehydrated and used

Mechanical Stress-induced Glutamate Signaling in PDL Cells

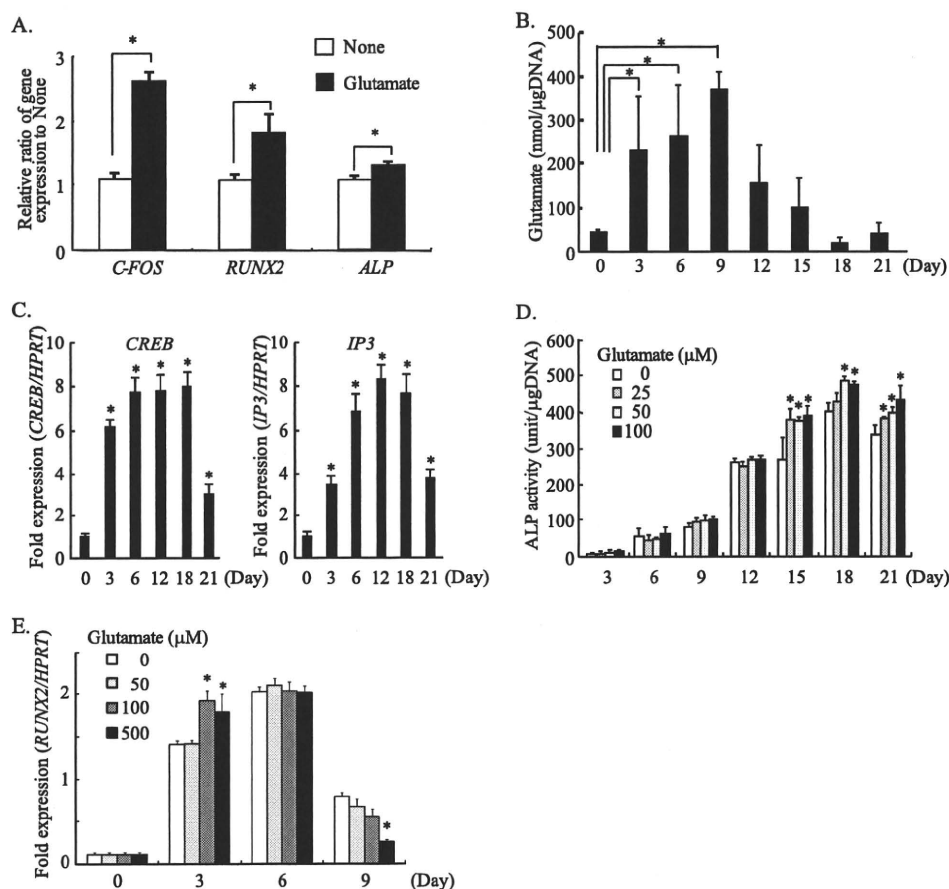


FIGURE 4. Functional analysis of glutamate signaling in human PDL cells. *A*, real-time RT-PCR was performed for the expressions of cytodifferentiation- and mineralization-related genes, such as *C-FOS*, *RUNX2*, and *ALP*, after a 12-h stimulation with exogenous glutamate (100 μ M). The expressions of *C-FOS*, *RUNX2*, and *ALP* were normalized by the *HPRT* expression. Values are shown as the relative ratios to the non-stimulated controls. Values represent the means \pm S.D. (error bars) of triplicate assays. Similar results were obtained in three separate experiments, and representative data are shown. $*$, $p < 0.05$, compared with PBS alone. *B*, human PDL cells were cultured in the mineralization-inducing medium. Every 3 days, the supernatants of the cultured cells were harvested, and the released glutamate was determined. Values represent the means \pm S.D. of triplicate assays. Similar results were obtained in three separate experiments, and representative data are shown. $*$, $p < 0.05$, compared with day 0. *C*, real-time RT-PCR was performed for the expressions of *CREB* and *IP₃* transcripts during the cytodifferentiation and mineralization of human PDL cells. The expressions of *CREB* and *IP₃* were normalized by the *HPRT* expression. Values are shown as the relative ratios to day 0. Values represent the means \pm S.D. of triplicate assays. Similar results were obtained in three separate experiments, and representative data are shown. $*$, $p < 0.01$, compared with day 0. *D*, human PDL cells were cultured in the mineralization-inducing medium in the presence of exogenous glutamate, followed by measurement of the ALP activities during the cytodifferentiation of human PDL cells. Values represent the means \pm S.D. of triplicate assays. Similar results were obtained in three separate experiments, and representative data are shown. $*$, $p < 0.05$, compared with 0 μ M glutamate. *E*, real-time RT-PCR was performed for the expression of *RUNX2* during the cytodifferentiation of human PDL cells. Values represent the means \pm S.D. of triplicate assays. Similar results were obtained in three separate experiments, and representative data are shown. $*$, $p < 0.05$, compared with 0 μ M glutamate.

for hybridization. Briefly, 0.5 μ g/ml of a DIG-UTP-labeled RNA probe was incubated at 85 $^{\circ}$ C for 3 min after dilution with hybridization solution, and the hybridization solution was then placed on the sections. The sections were covered with Parafilm and incubated at 52 $^{\circ}$ C for 16 h in a moist chamber saturated with 50% formamide. Next, the Parafilm was dislodged with 5 \times SSC at 50 $^{\circ}$ C, and the sections were sequentially incubated with 50% formamide in 2 \times SSC for 30 min at 52 $^{\circ}$ C and TNE buffer for 10 min. RNase A treatment (10 μ g/ml) was carried out at 37 $^{\circ}$ C in TNE buffer for 30 min. After washing with 2 \times SSC and 0.2 \times SSC twice for 15 min at 52 $^{\circ}$ C, the sections were incubated with DIG Buffer 1 for 2 min and then with 1.5% blocking re-

agent in DIG Buffer 1 for 60 min at room temperature. A 100 μ l/cm² specimen of diluted polyclonal sheep ALP-coupled anti-DIG Fab fragment (1:100–1:150) in DIG Buffer 1 was mounted on the sections and incubated for 30 min at room temperature. After the immunoreaction, the sections were washed twice with DIG Buffer 1 for 15 min and equilibrated with DIG Buffer 3 for 3 min. A coloring solution containing 337.5 μ g/ml nitro blue tetrazolium salt and 165 μ g/ml 5-bromo-4-chloro-3-indolyl-phosphate in DIG Buffer 3 was mounted on the sections and incubated at 4 $^{\circ}$ C for 12 h.

Statistical Analysis—Data were expressed as the mean \pm S.D. The statistical significance of differences between two means was examined by one-way analysis using Student's *t* test with the Bonferroni correction for multiple comparisons. *p* values of less than 0.05 were considered to indicate a significant difference.

RESULTS

Gene Expression Profile of Human PDL Cells under Mechanical Stress—First, we confirmed the application system of tensile mechanical stress to human PDL cells. After the application of tensile mechanical stress for 48 h, the axes of human PDL cells were aligned perpendicularly to the direction of the stretch force, whereas the control cells were aligned randomly (data not shown). To biologically evaluate whether the mechanical stress worked on human PDL cells in this system, we examined the gene expression of *C-FOS* (FB) murine osteosarcoma viral oncogene homolog), which is

known to be a mechanical stress-responsive gene (22). Real-time PCR analysis showed that the application of mechanical stress to human PDL cells for 48 h significantly up-regulated the gene expression of *C-FOS* (data not shown). Next, utilizing oligo-DNA chips, we analyzed the gene expression profile of human PDL cells after the application of mechanical stress for 48 h. The DNA chip analysis identified 17 up-regulated genes showing at least 2-fold differences in their relative intensities between the stretched cells and the non-stretched control cells (Fig. 1A). The full data are also accessible through the NCBI Gene Expression Omnibus (GEO) GSE19118. These results included the following genes with specific functions: for signal

Mechanical Stress-induced Glutamate Signaling in PDL Cells

transduction, *CNTFR* (ciliary neurotropic factor receptor) and *DSCR1* (Down syndrome critical region gene 1); for ECM remodeling, *MMP15* (matrix metalloproteinase 15); for ECM components, *LRRFIP1* (leucine-rich repeat interacting protein 1) and *MUC4* (mucin 4 cell surface-associated). Interestingly, we also identified two glutamate signaling-associated genes among the up-regulated genes: *HOMER1* (homer homolog 1) and *GRIN3A* (glutamate receptor ionotropic *N*-methyl-D-aspartate 3A). *HOMER1* is a glutamate receptor-binding protein, and *GRIN3A* is one of the glutamate receptor subunits. The *HOMER1* and *GRIN3A* mRNA expressions in the mechanically stressed human PDL cells were significantly up-regulated in the real-time PCR analysis (Fig. 1B).

Functional Expression of Glutamate Signaling-associated Molecules in Human PDL Cells—Glutamate receptors are divided into two groups: metabotropic G-protein-coupled receptors (mGluR1 to -8) and ionotropic ligand-gated channels. The ionotropic ligand-gated channels are subdivided into α -amino-3-hydroxy-5-methyl-4-isoxazole-propionate receptors (GRIA1 to -4), kainite receptors (GRIK1 to -5), and *N*-methyl-D-aspartate receptors (NMDARs; GRIN1, GRIN2A to -2D, GRIN3A, and GRIN3B) (23). Vesicular glutamate transporters (VGLUT1 to -3) (24) and adaptor molecules, such as *HOMER1*, also participate in glutamate signaling (25). Through our RT-PCR analysis, we found for the first time that human PDL cells constitutively expressed the mRNAs for *mGluR2* to -6, *GRIA3*, *GRIN1*, *GRIN2C*, *GRIN2D*, *GRIN3B*, and *VGLUT1* (Fig. 2A). Similar results were observed in human PDL cells derived from three different donors (data not shown). Next, we assessed whether the glutamate receptors were functional in human PDL cells. Determination of the intracellular Ca^{2+} influx showed that 100 μM exogenous glutamate apparently increased the fluorescence intensity compared with the control cells (Fig. 2B). These findings showed that exogenous glutamate induced an intracellular Ca^{2+} influx, followed by glutamate signaling in human PDL cells. We also analyzed the phosphorylation of CREB, which is mediated via mGluRs (26–28) and promotes the cytodifferentiation of osteoblasts *in vitro* and *in vivo* (29). Western blotting analysis showed that glutamate stimulation induced the phosphorylation of CREB in human PDL cells (Fig. 2C). These results indicated that the glutamate receptors expressed on human PDL cells were functional and that intracellular glutamate signal transduction was activated.

Effects of Mechanical Stress on Glutamate Signaling in Human PDL Cells—After the application of mechanical stress to human PDL cells for 24 h, we extracted total RNA and performed RT-PCR analyses. The analyses revealed that the mechanical stress up-regulated the gene expressions of *mGluR2*–6, *VGLUT1*, *GRIN1*, *GRIN2C*, and *GRIN3B* (Fig. 3A). Interestingly, we also found that human PDL cells spontaneously released glutamate and that the mechanical stress significantly increased the glutamate release after 48 h (Fig. 3B). We then assessed whether the mechanical stress induced the phosphorylation of CREB in human PDL cells. Western blotting analyses revealed that the mechanical stress induced the phosphorylation of CREB after 48 h (Fig. 3C).

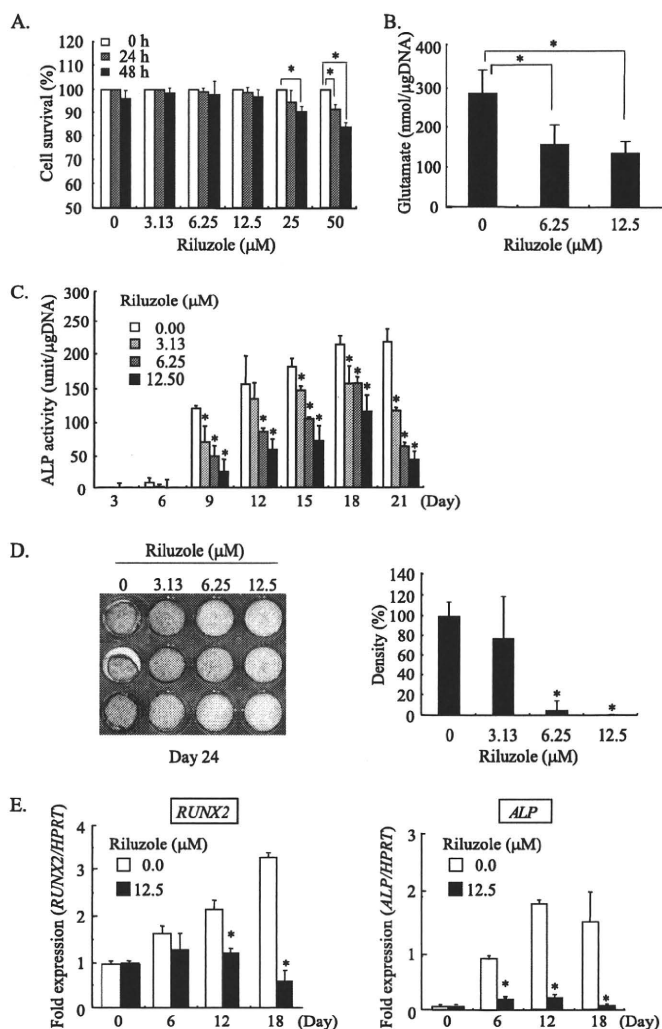


FIGURE 5. Effects of inhibition of glutamate release on the cytodifferentiation and mineralization of human PDL cells. A, the viabilities of human PDL cells were assessed after incubation in the presence or absence of riluzole for 0, 24, and 48 h. Values are shown as percentages relative to the numbers of surviving cells at 0 h. Values represent the means \pm S.D. (error bars) of triplicate assays. Similar results were obtained in three separate experiments, and representative data are shown. *, $p < 0.05$, compared with 0 h. B, human PDL cells were cultured in the mineralization-inducing medium in the presence or absence of riluzole for 24 days. The release of glutamate from human PDL cells was measured on day 9. C, the ALP activities were analyzed. D, the mineralized nodule formation was analyzed on day 24. A picture of the alizarin red staining is shown on the left, and the densities of the alizarin red staining analyzed by the software Win ROOF are shown on the right. E, total RNA was extracted from human PDL cells during the cytodifferentiation and mineralization of the cells. Real-time RT-PCR was performed for the gene expressions of *RUNX2* and *ALP*. The *RUNX2* and *ALP* expressions were normalized by the *HPRT* expression. Values represent the means \pm S.D. of triplicate assays. Similar results were obtained in three separate experiments, and representative data are shown. *, $p < 0.05$, compared with 0 μM riluzole.

Functional Analysis of Glutamate Signaling in Human PDL Cells—As shown in Fig. 4A, glutamate stimulation of human PDL cells up-regulated the gene expressions of *C-FOS*, *ALP*, and *RUNX2* (Runt-related transcription factor 2), which are known to be cytodifferentiation- and mineralization-related genes. These findings suggest the involvement of glutamate signaling in the cytodifferentiation and mineralization of human PDL cells. Thus, we measured the release of glutamate during the cytodifferentiation of human PDL cells into mineralized tissue-forming cells. We confirmed that the ALP activities

Mechanical Stress-induced Glutamate Signaling in PDL Cells

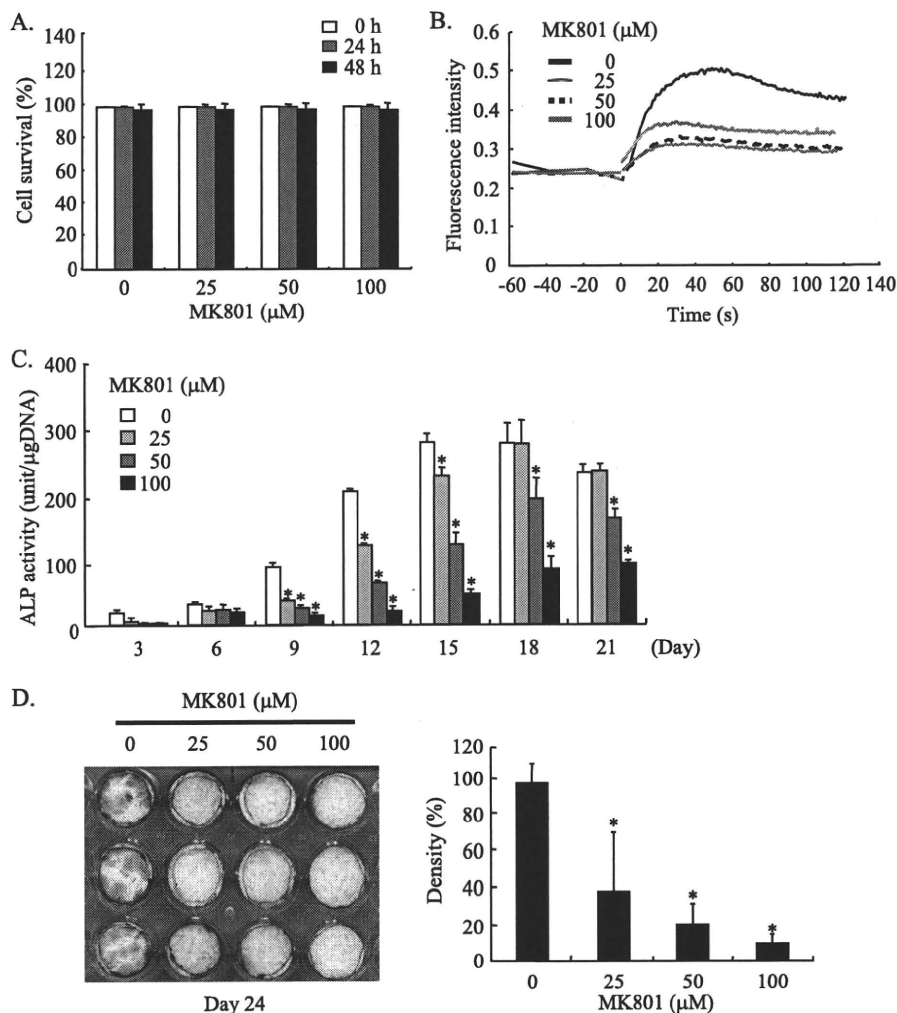


FIGURE 6. Effects of inhibition of glutamate signaling via NMDARs on the cytodifferentiation and mineralization of human PDL cells. *A*, the viabilities of human PDL cells were assessed after incubation in the presence or absence of MK801 for 0, 24, and 48 h. Values are shown as percentages relative to the numbers of the surviving cells at 0 h. Values represent the means \pm S.D. (error bars) of triplicate assays. Similar results were obtained in three separate experiments, and representative data are shown. *B*, the Ca^{2+} influxes in human PDL cells in the presence or absence of MK801 were determined after stimulation of human PDL cells with 100 μM exogenous glutamate. The fluorescence intensity was measured to assess the Ca^{2+} influx into human PDL cells. Zero seconds indicates the time of the stimulation with glutamate. A representative experiment of four independent experiments is shown. *C*, human PDL cells were cultured in the mineralization-inducing medium in the presence or absence of MK801, and the ALP activities were measured. *D*, the mineralized nodule formation was analyzed on day 24. A picture of the alizarin red staining is shown on the left, and the densities of the alizarin red staining analyzed by the software Win ROOF are shown on the right. Values represent the means \pm S.D. of triplicate assays. Similar results were obtained in three separate experiments, and representative data are shown. *, $p < 0.05$, compared with 0 μM MK801.

gradually increased during culture of human PDL cells in the mineralization-inducing medium for 21 days (data not shown). Under these experimental conditions, the release of glutamate from human PDL cells was increased during the process of the cytodifferentiation and reached its peak on day 9 of long term culture (Fig. 4B). Next, we assessed the expressions of CREB and inositol 1,4,5-trisphosphate (IP_3), which is one of second messengers of glutamate signaling via mGluRs (26). Real-time PCR analyses revealed up-regulation of CREB and IP_3 during the cytodifferentiation of PDL cells with the exact same pattern of glutamate secretion (Fig. 4C). These results suggested that glutamate secreted by PDL cells induces CREB and IP_3 expressions during the course of the cytodifferentiation. Subsequently, we examined the effect of the exogenous addition of

glutamate on the cytodifferentiation of human PDL cells. As shown in Fig. 4D, the ALP activities of human PDL cells were significantly enhanced by the addition of glutamate for 15 days after the induction of the cytodifferentiation of human PDL cells. *RUNX2* expression was also significantly enhanced by the addition of glutamate during the early stage of the cytodifferentiation of human PDL cells (Fig. 4E). These results suggest that glutamate signaling is involved in the cytodifferentiation of human PDL cells into mineralized tissue-forming cells.

Effects of Inhibition of Glutamate Release on the Cytodifferentiation and Mineralization of Human PDL Cells—To investigate the effects of endogenous glutamate signaling on the cytodifferentiation and mineralization of human PDL cells, we utilized a glutamate release inhibitor, riluzole. First, we examined the effect of riluzole on the survival of human PDL cells. The cell survival assay showed that riluzole at 12.5 μM or less did not affect the viability of human PDL cells after a 48-h incubation (Fig. 5A). We then confirmed the effect of riluzole on the inhibition of glutamate release from human PDL cells. As shown in Fig. 5B, we found that riluzole significantly decreased the glutamate release from human PDL cells during the cytodifferentiation in a dose-dependent manner.

To examine the effects of riluzole on the cytodifferentiation and mineralization of human PDL cells, we cultured human PDL cells in the mineralization-inducing medium in

the presence of riluzole. Riluzole significantly decreased the ALP activities during the cytodifferentiation of human PDL cells in a dose-dependent manner (Fig. 5C). The results of alizarin red staining also showed that riluzole inhibited the mineralized nodule formation on day 24 during the course of the cytodifferentiation of human PDL cells in a dose-dependent manner (Fig. 5D). In addition, real-time RT-PCR analysis revealed that riluzole significantly down-regulated the gene expressions of *RUNX2* and *ALP* during the cytodifferentiation of human PDL cells (Fig. 5E).

Effects of Inhibition of Glutamate Signaling via NMDARs on the Cytodifferentiation and Mineralization of Human PDL Cells—NMDARs are specific glutamate ionotropic receptors and are composed of heteromeric assemblies between the

Mechanical Stress-induced Glutamate Signaling in PDL Cells

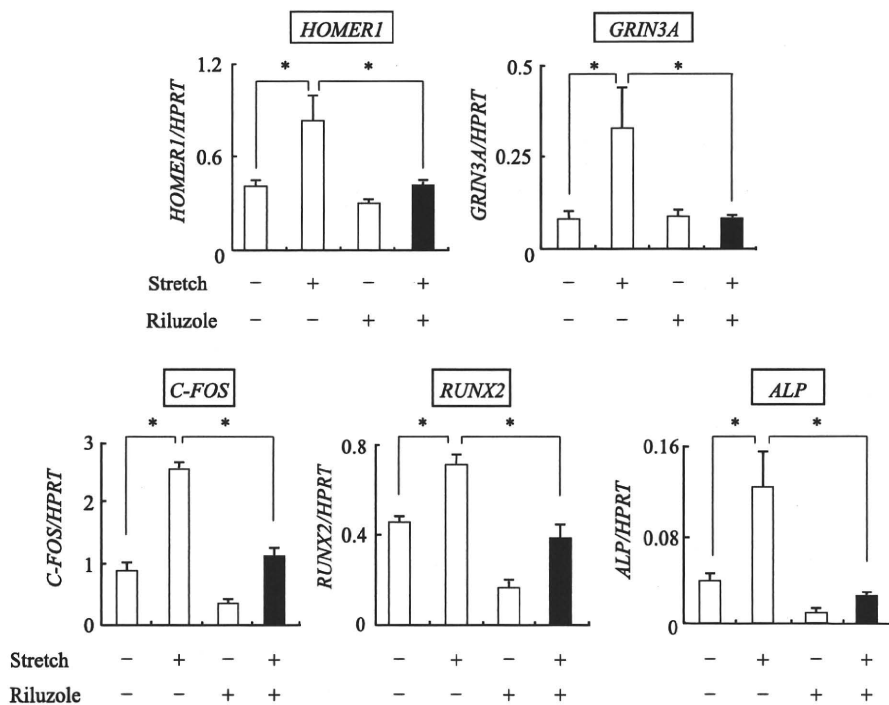


FIGURE 7. Effects of glutamate signaling on mechanical stress-induced gene expressions. Real-time RT-PCR was performed for the gene expressions of *HOMER1*, *GRIN3A*, *C-FOS*, *RUNX2*, and *ALP* in human PDL cells after the application of mechanical stress for 48 h in the presence or absence of riluzole (12.5 μM). Each gene expression was normalized by the *HPRT* expression. Values represent the means \pm S.D. (error bars) of triplicate assays. Similar results were obtained in three separate experiments, and representative data are shown. *, $p < 0.05$.

essential *GRIN1* subunit and the other subunits (30, 31). These receptors play an important role in the initiation of neuroplasty and modulate intracellular Ca^{2+} influx, activate Ca^{2+} -dependent enzymes such as Ca^{2+} /calmodulin-dependent protein kinases (CaMKII) and calcineurin, and regulate the phosphorylation of proteins and gene transcription (32).

To analyze the effects of glutamate signaling via NMDARs on the cytodifferentiation and mineralization of human PDL cells, we utilized an antagonist of NMDARs, MK801. First, we examined the effect of MK801 on the survival of human PDL cells. The cell survival assay revealed that MK801 at 100 μM or less had no effect on the viability of human PDL cells after a 48-h incubation (Fig. 6A). Human PDL cells were stimulated with 100 μM exogenous glutamate in the presence of MK801 to confirm the antagonistic effect of MK801 on the activation of NMDARs in human PDL cells. Determination of the Ca^{2+} influx showed that MK801 inhibited the fluorescence intensity in a dose-dependent manner (Fig. 6B).

To examine the effects of MK801 on the cytodifferentiation and mineralization of human PDL cells, we cultured human PDL cells in the mineralization-inducing medium in the presence of MK801. As shown in Fig. 6C, MK801 significantly suppressed the ALP activities in a dose-dependent manner during the cytodifferentiation of human PDL cells. Alizarin red staining revealed that MK801 significantly reduced the mineralized nodule formation on day 24 during the course of the cytodifferentiation and mineralization of human PDL cells (Fig. 6D).

Effects of Glutamate Signaling on Mechanical Stress-induced Gene Expression—To analyze the relationships among glutamate signaling, mechanical stress, and the cytodifferentiation

and mineralization of human PDL cells, we examined the effects of riluzole on the cytodifferentiation and mineralization-related gene expressions in human PDL cells under mechanical stress. Real-time RT-PCR analyses demonstrated that the gene expressions of *HOMER1* and *GRIN3A* were up-regulated after a 48-h mechanical stress in the absence of riluzole. On the other hand, riluzole significantly inhibited the up-regulation of the *HOMER1* and *GRIN3A* expressions (Fig. 7, upper panels). Likewise, the mechanical stress-induced gene expressions of *C-FOS*, *RUNX2*, and *ALP* as cytodifferentiation and mineralization-related genes were also down-regulated in the presence of riluzole (Fig. 7, bottom).

In Vivo Induction of the Gene Expressions of Glutamate Signaling-associated Molecules in PDL Tissue by Orthodontic Tooth Movement—To establish the biological relevance of the *in vitro* studies to the *in vivo* situation, we investigated the gene

expressions of the glutamate signaling-associated molecules in PDL tissue by utilizing a mouse model of orthodontic tooth movement (21). We selected probes for *Homer1*, *Vglut1*, *Grin1*, *mGluR3*, *mGluR5*, and *mGluR6*. The upper molar teeth were moved by an orthodontic force mediated by a closed-coil spring for 0, 12, and 24 h. We observed horizontal cross-sections of the tooth roots at the indicated time points by hematoxylin-eosin (H&E) staining (Fig. 8A, a–c). At 12 and 24 h after the application, the root was moving to the right side in each image. In Fig. 8, tension sites were created on the left side of the root, and pressure sites were present on the right side. At the indicated time points, the teeth were moving in the direction of the force within the dental sockets, and resorption and remodeling of the alveolar bone were initially activated (Fig. 8A, a–c). *In situ* hybridization analyses revealed that the PDL faintly expressed the glutamate signaling-associated molecule genes *Homer1*, *Vglut1*, *Grin1*, *mGluR3*, *mGluR5*, and *mGluR6* at the base line (Fig. 8A, d, g, j, m, p, and s). Of note was the observation that these gene expressions were up-regulated at the tension sites at 12 and 24 h after the application (Fig. 8A, e, f, h, i, k, l, n, o, q, r, t, and u). On the contrary, the mRNA expression levels of these molecules were not changed at the pressure sites at 12 and 24 h after the application (Fig. 8A, e, f, h, i, k, l, n, o, q, r, t, and u). We also analyzed the expressions of the cytodifferentiation and mineralization-related genes *Runx2*, type I collagen, and osteocalcin. *In situ* hybridization analyses revealed that the mRNA expression of *Runx2* was observed even in normal PDL cells (at 0 h) and thereafter was only increased at the tension sites after the application of orthodontic force (Fig. 8B, a–c). This finding indicated that cytodifferentiation of PDL cells at the tension

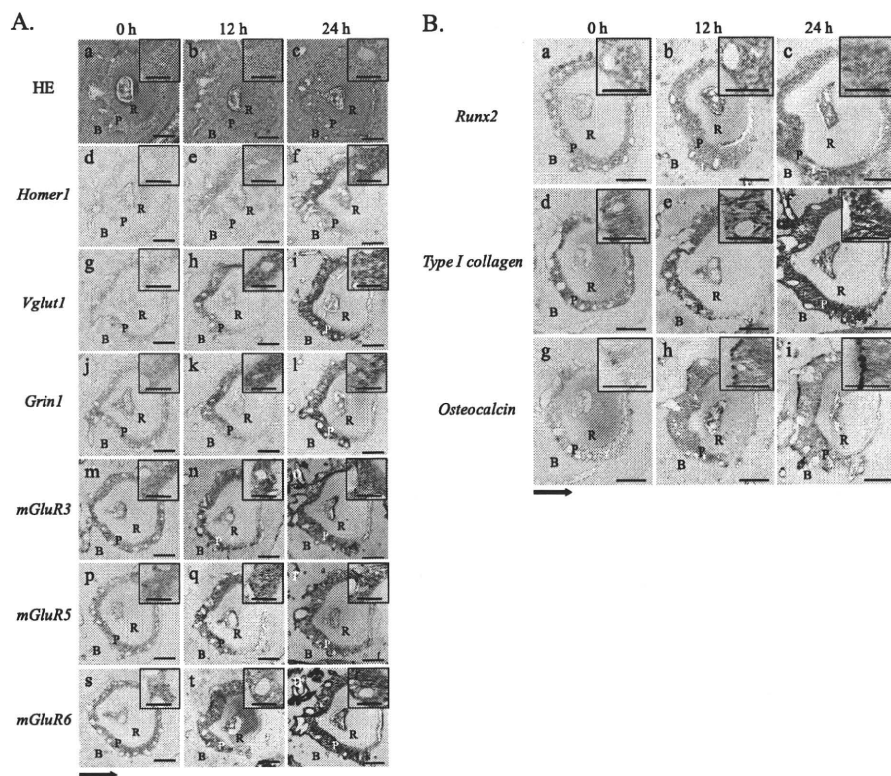


FIGURE 8. *In vivo* induction of the gene expressions of glutamate signaling-associated molecules in PDL tissue by orthodontic tooth movement. The upper first molars of ICR mice were moved with orthodontic force for the indicated time periods. Horizontal sections of the periodontium around the palatal root of the first molars were stained. *A*, H&E staining (*a–c*). The gene expressions of *Homer1* (*d–f*), *Vglut1* (*g–i*), *Grin1* (*j–l*), *mGluR3* (*m–o*), *mGluR5* (*p–r*), and *mGluR6* (*s–u*) were analyzed by *in situ* hybridization. *B*, the gene expressions of the cytodifferentiation and mineralization-related genes *Runx2* (*a–c*), type I collagen (*d–f*), and osteocalcin (*g–i*) were analyzed by *in situ* hybridization. P, PDL; R, root; B, bone. Scale bars, 200 μ m. Black arrow, direction of the force application. Each inset shows a higher magnification image of the tension sites (left side). Scale bars in the insets, 100 μ m.

sites was induced by the mechanical stress *in vivo*. Type I collagen was also expressed in the PDL at 0 h and then clearly up-regulated at the tension sites (Fig. 8*B*, *d–f*), indicating active synthesis of collagen fibers. Moreover, strong expression of osteocalcin was detected near the alveolar bone at the tension sites after 24 h of the force application (Fig. 8*B*, *g–i*), showing that bone remodeling was activated by mechanical tensile stress *in vivo*.

DISCUSSION

Mechanical stress is one of the most important factors for maintaining the homeostasis of a variety of tissues, such as bone, muscle, skin, and blood vessels. PDL tissues are also influenced and regulated by mechanical stresses, such as occlusal pressure and orthodontic forces. The physiological levels of the forces regulate cellular functions and remodeling of the PDL adequately, whereas pathophysiological forces can induce connective tissue destruction and bone and teeth resorption in periodontal diseases or inadequate orthodontic tooth treatments clinically.

The signaling pathways linking mechanical stress to cell functions are still not well described. In the present study, we carried out a comprehensive microarray analysis to assess the influences of physiological tensile mechanical stress on human PDL cells *in vitro* and identified the up-regulation of glutamate signaling-associated genes.

We further revealed that a mechanical stretch applied to human PDL cells induced their cytodifferentiation and mineralization through activation of glutamate signaling pathways.

In this study, we identified 17 up-regulated genes, including *CNTFR*, *DSCR1*, *MMP15*, *LRRFIP1*, *PLXND1*, and *ANGPTL1*, in human PDL cells after a 48-h mechanical stress using a DNA chip analysis. Interestingly, de Araujo *et al.* (33) reported a microarray analysis of human PDL cells under compressive forces using an *in vitro* three-dimensional culture system. They identified several up-regulated genes, including inflammation-related molecules, such as *COX-2* (cyclooxygenase-2), *PGE₂* (prostaglandin E₂), *IL-6* (interleukin-6), and *IL-1 β* (interleukin-1 β), which were not listed in our present study. These findings suggest that mechanical compressive stress tends to induce inflammation and destructive responses, whereas tensile stress induces cytodifferentiation and remodeling responses in PDL cells *in vivo*, similar to those in orthodontic treatments. *CNTFR* encodes a receptor for ciliary neuro-

tropic factor, which is known to be a growth factor. Ciliary neurotropic factor has been implicated in the regulation of cell survival and cytodifferentiation in the brain (34). *DSCR1*, the product of a chromosome 21 gene highly expressed in the brain, is located in the minimal candidate region for the Down syndrome phenotype. *DSCR1* protein encoded by the gene interacts with calcineurin A to inhibit calcineurin-dependent signaling pathways and induce anti-inflammatory reactions (35). *MMP15* is a member of the matrix metalloproteinase (MMP) family and promotes ECM remodeling (36). *LRRFIP1* (leucine-rich repeat (in FLII)-interacting protein 1), which is an ECM component, occupies a tumor necrosis factor- α (TNF- α) promoter site and appears to act as a repressor of TNF- α production (37). *PLXND1* (Plexin D1) (38) and *ANGPTL1* (angiopoietin-like 1) (39) are both associated with vasculogenesis and angiogenesis. In summary, the differentiation, proliferation, ECM remodeling, and angiogenesis induced by mechanical stress may contribute to arranging the optimal microcircumstances for the homeostasis and remodeling of PDL tissue. Among these up-regulated genes, we found two glutamate signaling-associated genes, *HOMER1* and *GRIN3A*. *HOMER1* encodes a member of the homer family of dendritic proteins and regulates intracellular Ca²⁺. *HOMER* connects group 1 mGluRs, such as mGluR1 and mGluR5, to other scaffolding proteins (40). *GRIN3A* encodes a subunit of NMDAR, which

Mechanical Stress-induced Glutamate Signaling in PDL Cells

belongs to the superfamily of glutamate-regulated ion channels. Further analyses revealed that in addition to *HOMER1* and *GRIN3A*, human PDL cells constitutively and functionally expressed glutamate signaling-associated molecules, including glutamate and its receptors. We also demonstrated that the application of mechanical stress to human PDL cells up-regulated the expressions of glutamate signaling-associated genes, increased the secretion of glutamate from the cells, and induced intracellular signal transduction. These results reveal that mechanical stress activates glutamate signaling pathways in human PDL cells.

Recently, glutamate signaling has been reported to be involved in bone metabolism (41). There are some similarities between PDL cells and osteoblasts, in that PDL cells can differentiate into mineralized tissue-forming cells when they are cultured in mineralization-inducing medium *in vitro* (42). The induction of the cytodifferentiation of human PDL cells increased the release of glutamate from human PDL cells as well as CREB and IP₃ transcription. Exogenous glutamate enhanced the ALP activities and *RUNX2* expression during the cytodifferentiation of human PDL cells. These results suggest that glutamate signaling promotes the cytodifferentiation and mineralization of human PDL cells. The suppression of ALP activities and calcified nodule formation of human PDL cells by riluzole, an inhibitor of glutamate release, and MK801, an antagonist of NMDARs, strengthens the notion that glutamate signaling is crucial for the cytodifferentiation and mineralization of human PDL cells. The analyses utilizing MK801 suggested that glutamate signaling via NMDARs contributes to the enhancement of the cytodifferentiation and mineralization of human PDL cells. The effects of antagonists for other glutamate receptors on the cytodifferentiation and mineralization of human PDL cells warrant further investigation.

Mechanical stress has been reported to induce the expressions of cytodifferentiation and mineralization-related genes in osteoblasts (43). However, the molecular mechanism of the activation of osteoblasts that leads to bone remodeling has not been fully elucidated. In this study, we confirmed that human PDL cells up-regulated the gene expressions of *C-FOS*, *RUNX2*, and *ALP* under mechanical stress. On the other hand, riluzole inhibited the up-regulation of the mechanical stress-induced gene expressions of *C-FOS*, *RUNX2*, and *ALP*. These results suggest that glutamate signaling controls the upstream of the mechanical stress-induced gene expressions and clearly demonstrate the involvement of glutamate signaling in the mechanical stress-induced cytodifferentiation and mineralization of human PDL cells.

Orthodontic tooth movement has been defined as the result of biological responses to mechanical stress applied to a tooth and is achieved by PDL and alveolar bone remodeling. Bone formation and resorption are induced at the tension sites and pressure sites, respectively. The *in situ* hybridization analyses revealed that the expressions of the glutamate signaling-associated genes *Homer1*, *Vglut1*, *Grin1*, *mGluR3*, *mGluR5*, and *mGluR6* were clearly up-regulated in the tension sites of the PDL under orthodontic tooth movement *in vivo*. Up-regulation of the cytodifferentiation and mineralization-related genes *Runx2*, type I collagen, and osteocalcin was observed in the

tension sites. These findings strongly support our *in vitro* data indicating that glutamate signaling was induced by the tensile mechanical stress and promoted the cytodifferentiation and mineralization of PDL cells. According to a previous report that tensile force activates PDL cells and modulates PDL remodeling by the induction of ECM synthesis and degradation (32), we consider that the glutamate signaling-associated molecules are also modulated together with the activation of PDL cells and PDL remodeling in response to mechanical stress.

In conclusion, we have demonstrated that mechanical stress induces glutamate signaling in the PDL, resulting in enhancement of the cytodifferentiation and mineralization of PDL cells. These findings suggest that mechanical stress-induced glutamate signaling is involved in the homeostasis, remodeling, and regeneration of periodontal tissue.

Acknowledgments—We thank Dr. Kaori Izutsu and Dr. Tetsuya Iida (Laboratory of Genomic Research on Pathogenic Bacteria, International Research Center for Infectious Diseases, Research Institute for Microbial Diseases, Osaka University, Japan) for technical support for the scanning and analysis of the DNA chips.

REFERENCES

1. Wang, J. H., and Thampatty, B. P. (2006) *Biomech. Model Mechanobiol.* **5**, 1–16
2. Henneman, S., Bildt, M. M., Degroot, J., Kuijpers-Jagtman, A. M., and Von den Hoff, J. W. (2008) *Arch. Oral Biol.* **53**, 161–167
3. Ozaki, S., Kaneko, S., Podyma-Inoue, K. A., Yanagishita, M., and Soma, K. (2005) *J. Periodontol. Res.* **40**, 110–117
4. Takano-Yamamoto, T., Takemura, T., Kitamura, Y., and Nomura, S. (1994) *J. Histochem. Cytochem.* **42**, 885–896
5. Domon, S., Shimokawa, H., Yamaguchi, S., and Soma, K. (2001) *Eur. J. Orthod.* **23**, 339–348
6. Pavlin, D., and Gluhak-Heinrich, J. (2001) *Crit. Rev. Oral Biol. Med.* **12**, 414–424
7. Vignery, A., and Baron, R. (1980) *Anat. Rec.* **196**, 191–200
8. Cohn, S. A. (1965) *Arch. Oral Biol.* **10**, 909–919
9. Kaneko, S., Ohashi, K., Soma, K., and Yanagishita, M. (2001) *J. Periodontol. Res.* **36**, 9–17
10. Hollmann, M., O'Shea-Greenfield, A., Rogers, S. W., and Heinemann, S. (1989) *Nature* **342**, 643–648
11. Torii, K., and Cagan, R. H. (1980) *Biochim. Biophys. Acta.* **627**, 313–323
12. Bertrand, G., Gross, R., Puech, R., Loubatières-Mariani, M. M., and Bocckaert, J. (1992) *Br. J. Pharmacol.* **106**, 354–359
13. Patton, A. J., Genever, P. G., Birch, M. A., Suva, L. J., and Skerry, T. M. (1998) *Bone* **22**, 645–649
14. Skerry, T. M., and Genever, P. G. (2001) *Trends Pharmacol. Sci.* **22**, 174–181
15. Somerman, M. J., Archer, S. Y., Imm, G. R., and Foster, R. A. (1988) *J. Dent. Res.* **67**, 66–70
16. Matsuda, N., Yokoyama, K., Takeshita, S., and Watanabe, M. (1998) *Arch. Oral Biol.* **43**, 987–997
17. Nicholls, D. G., and Sihra, T. S. (1986) *Nature* **321**, 772–773
18. Bessay, O. A., Lowry, O. H., and Brock, M. J. (1946) *J. Biol. Chem.* **164**, 321–329
19. Labarca, C., and Paigen, K. (1980) *Anal. Biochem.* **102**, 344–352
20. Dahl, L. K. (1952) *Proc. Soc. Exp. Biol. Med.* **80**, 474–479
21. Sakai, Y., Balam, T. A., Kuroda, S., Tamamura, N., Fukunaga, T., Takigawa, M., and Takano-Yamamoto, T. (2009) *J. Dent. Res.* **88**, 345–350
22. Yamaguchi, N., Chiba, M., and Mitani, H. (2002) *Arch. Oral Biol.* **47**, 465–471
23. Wisden, W., and Seeburg, P. H. (1993) *Curr. Opin. Neurobiol.* **3**, 291–298
24. Moriyama, Y., and Yamamoto, A. (2004) *J. Biochem.* **135**, 155–163

Mechanical Stress-induced Glutamate Signaling in PDL Cells

25. Ango, F., Robbe, D., Tu, J. C., Xiao, B., Worley, P. F., Pin, J. P., Bockaert, J., and Fagni, L. (2002) *Mol. Cell. Neurosci.* **20**, 323–329
26. Niswender, C. M., and Conn, P. J. (2010) *Annu. Rev. Pharmacol. Toxicol.* **50**, 295–322
27. Mao, L., and Wang, J. Q. (2003) *J. Neurochem.* **84**, 233–243
28. Harris, S. L., Cho, K., Bashir, Z. I., and Molnar, E. (2004) *Mol. Cell. Neurosci.* **25**, 275–287
29. Siddappa, R., Martens, A., Doorn, J., Leusink, A., Olivo, C., Licht, R., van Rijn, L., Gaspar, C., Fodde, R., Janssen, F., van Blitterswijk, C., and de Boer, J. (2008) *Proc. Natl. Acad. Sci. U.S.A.* **105**, 7281–7286
30. Iemata, M., Takarada, T., Hinoi, E., Taniura, H., and Yoneda, Y. (2007) *J. Cell. Physiol.* **213**, 721–729
31. Monyer, H., Sprengel, R., Schoepfer, R., Herb, A., Higuchi, M., Lomeli, H., Burnashev, N., Sakmann, B., and Seeburg, P. H. (1992) *Science* **256**, 1217–1221
32. Malenka, R. C., and Nicoll, R. A. (1999) *Science* **285**, 1870–1874
33. de Araujo, R. M., Oba, Y., and Moriyama, K. (2007) *J. Periodontal Res.* **42**, 15–22
34. Müller, S., Chakrapani, B. P., Schwegler, H., Hofmann, H. D., and Kirsch, M. (2009) *Stem Cells* **27**, 431–441
35. Fuentes, J. J., Genescà, L., Kingsbury, T. J., Cunningham, K. W., Pérez-Riba, M., Estivill, X., and de la Luna, S. (2000) *Hum. Mol. Genet.* **9**, 1681–1690
36. English, J. L., Kassiri, Z., Koskivirta, I., Atkinson, S. J., Di Grappa, M., Soloway, P. D., Nagase, H., Vuorio, E., Murphy, G., and Khokha, R. (2006) *J. Biol. Chem.* **281**, 10337–10346
37. Suriano, A. R., Sanford, A. N., Kim, N., Oh, M., Kennedy, S., Henderson, M. J., Dietzmann, K., and Sullivan, K. E. (2005) *Mol. Cell. Biol.* **25**, 9073–9081
38. Kanda, T., Yoshida, Y., Izu, Y., Nifuji, A., Ezura, Y., Nakashima, K., and Noda, M. (2007) *J. Cell. Biochem.* **101**, 1329–1337
39. Lai, D. M., Li, H., Lee, C. C., Tzeng, Y. S., Hsieh, Y. H., Hsu, W. M., Hsieh, F. J., Cheng, J. T., and Tu, Y. K. (2008) *Neurochem. Int.* **52**, 470–477
40. Roche, K. W., Tu, J. C., Petralia, R. S., Xiao, B., Wenthold, R. J., and Worley, P. F. (1999) *J. Biol. Chem.* **274**, 25953–25957
41. Chenu, C., Serre, C. M., Raynal, C., Burt-Pichat, B., and Delmas, P. D. (1998) *Bone* **22**, 295–299
42. Piche, J. E., Carnes, D. L., Jr., and Graves, D. T. (1989) *J. Dent. Res.* **68**, 761–767
43. Nomura, S., and Takano-Yamamoto, T. (2000) *Matrix Biol.* **19**, 91–96

Fibroblast Growth Factor-2 Stimulates Directed Migration of Periodontal Ligament Cells via PI3K/AKT Signaling and CD44/Hyaluronan Interaction

YOSHIO SHIMABUKURO, HIROAKI TERASHIMA, MASAHIDE TAKEDACHI, KENICHIRO MAEDA, TOMOMI NAKAMURA, KEIGO SAWADA, MARIKO KOBASHI, TOSHIHITO AWATA, HIROYUKI OOHARA, TAKANOBU KAWAHARA, TOMOAKI IWAYAMA, TOMOKO HASHIKAWA, MANABU YANAGITA, SATORU YAMADA, AND SHINYA MURAKAMI*

Division of Oral Biology and Disease Control, Department of Periodontology, Osaka University Graduate School of Dentistry, Osaka, Japan

Fibroblast growth factor-2 (FGF-2) regulates a variety of functions of the periodontal ligament (PDL) cell, which is a key player during tissue regeneration following periodontal tissue breakdown by periodontal disease. In this study, we investigated the effects of FGF-2 on the cell migration and related signaling pathways of MPDL22, a mouse PDL cell clone. FGF-2 activated the migration of MPDL22 cells and phosphorylation of phosphatidylinositol 3-kinase (PI3K) and akt. The PI3K inhibitors, Wortmannin and LY294002, suppressed both cell migration and akt activation in MPDL22, suggesting that the PI3K/akt pathway is involved in FGF-2-stimulated migration of MPDL22 cells. Moreover, in response to FGF-2, MPDL22 showed increased CD44 expression, avidity to hyaluronan (HA) partly via CD44. HA production and mRNA expression of HA synthase (Has)-1, 2, and 3. However, the distribution of HA molecular mass produced by MPDL22 was not altered by FGF-2 stimulation. Treatment of transwell membrane with HA facilitated the migration of MPDL22 cells and an anti-CD44 neutralizing antibody inhibited it. Interestingly, the expression of CD44 was colocalized with HA on the migrating cells when stimulated with FGF-2. Furthermore, an anti-CD44 antibody and small interfering RNA for CD44 significantly decreased the FGF-2-induced migration of MPDL22 cells. Taken together, PI3K/akt and CD44/HA signaling pathways are responsible for FGF-2-mediated cell motility of PDL cells, suggesting that FGF-2 accelerates periodontal regeneration by regulating the cellular functions including migration, proliferation and modulation of extracellular matrix production.

J. Cell. Physiol. 226: 809–821, 2011. © 2010 Wiley-Liss, Inc.

Cell migration is essential for embryogenesis, tissue development, wound healing, and tissue regeneration. This cellular event requires coordinated multiple processes such as activation of related signaling pathways, membrane-linked cytoskeleton reorganization, causing specific structural changes in the plasma membrane, and interaction with the extracellular matrix.

Phosphatidylinositol 3-kinase (PI3K) is associated with cell polarization and migration in a wide range of cell types (Derman et al., 1997; Ren and Schwartz, 1998; Cantley, 2002; Weiner et al., 2002). Polarized accumulation of phospholipid PI(3,4,5)P₃ and its product is seen via PI3K for establishment of cell polarity and migration during chemotaxis. In addition, PI3K and its downstream kinase effector akt are known to regulate cytoskeletal rearrangements, cell migration, apoptosis, and other biological functions.

As one of the key extracellular matrices involved in cell migration, hyaluronan (HA) has been receiving particular attention. HA is a linear glycosaminoglycan composed of repeating disaccharides of glucuronic acid and *N*-acetylglucosamine: [β 1,4-GlcUA- β 1,3-GlcNAc-] and is ubiquitously distributed in the body. HA is synthesized at the inner face of the plasma membrane by HA synthase (Has). A wide variety of mediators regulate the HA synthesis and in turn modulate physiological and pathophysiological conditions via HA. So far, HA has been reported to be involved in not only matrix organization, but also cell adherence, cell migration, cell proliferation. In the early phase of tissue repair, enhanced expression of HA precedes other glycosaminoglycan (Lammi

et al., 2001), leading to facilitation of cell motility and subsequent tissue remodeling.

CD44, a cell surface molecule, is one of the major receptors for HA. The intracellular portion is linked to actin filaments and mediates intracellular signal transduction. Interestingly, CD44 has been reported to be present on the leading edge of migrating cells (Thorne et al., 2004). The interaction of CD44 with HA activates Rac1 and in turn regulates the formation of cytoskeleton-mediated membrane protrusions and cell migration (Bourguignon et al., 2000). Myoblasts derived from CD44-deficient mouse lacked the chemotaxis seen in the wild-type myoblasts (Mylona et al., 2006). In addition, CD44-deficient fibroblasts revealed less directional migration and less efficiency of wound closure in wound healing assay in spite of the increased motility compared with the wild type (Acharya

Contract grant sponsor: Research Fellow of the Japan Society for the Promotion of Science;

Contract grant numbers: 20390529, 20390530, 20592427, 21592623, 21659482, 21890137, 22592182.

*Correspondence to: Shinya Murakami, 1-8 Yamadaoka, Suita, Osaka 565-0871, Japan. E-mail: ipshinya@dent.osaka-u.ac.jp

Received 15 October 2009; Accepted 17 August 2010

Published online in Wiley Online Library (wileyonlinelibrary.com), 20 September 2010.

DOI: 10.1002/jcp.22406